nature climate change

Article

https://doi.org/10.1038/s41558-026-02686-x

Multi-centennial response of marine carbon pumps to global warming

Received: 22 May 2025

Accepted: 4 June 2026

Published online: 25 June 2026

Check for updates

Samar Khatiwala [1] ✉, Olivia Strachan [2] & Andreas Schmittner [3]

The ocean's capacity to absorb anthropogenic CO_2 is predicted to decrease with global warming, reinforcing a climate–carbon cycle feedback. However, the effects of specific mechanisms such as circulation and temperature on marine carbon components and atmospheric CO_2 under future emission scenarios remain poorly quantified, especially on multi-centennial timescales. Here, using a decomposition of dissolved inorganic carbon, we show that under high-emission scenarios, circulation changes dominate the climate–carbon cycle feedback by reducing anthropogenic carbon uptake and redistributing alkalinity, despite compensating increases in biological carbon storage and air–sea disequilibrium. By contrast, under low emissions, temperature changes, amplified by increased physical disequilibrium, dominate the climate–carbon cycle feedback. Previous estimates using the apparent oxygen utilization approximation may have considerably underestimated changes in biological carbon storage. These results improve mechanistic understanding of long-term global carbon cycle dynamics, with implications for efforts to achieving zero net emissions and proposed marine CO_2 removal strategies.

The cycling of carbon in the ocean is controlled by different physical, chemical and biological processes[1], complicating the interpretation and attribution of observed and modelled changes. Air–sea gas exchange tends to equilibrate surface ocean pCO_2 with the atmosphere (pCO_2^{atm}) and thus affects climate. In sea water, CO_2 dissociates into bicarbonate and carbonate ions, which provides buffering capacity and increases dissolved inorganic carbon (DIC), which dominates ocean carbon storage and is the focus of this Article. There are two carbon 'pumps'[2] that act to concentrate DIC in deeper layers, thus reducing surface and atmospheric CO_2 (ref. 2). The solubility pump results from higher solubility of CO_2 in cold waters of polar origin and increases physical carbon storage, while the biological pump is associated with biological production of organic carbon and calcium carbonate at the surface and their sinking and regeneration into DIC at depth. We refer to DIC of this origin as C_{soft} and C_{caco3}, respectively, and their sum as C_{reg}. Ocean circulation moves elevated subsurface DIC back to the surface, completing the 'loop' and exposing it to air–sea gas exchange.

Fossil fuel burning has increased pCO_2^{atm}, with the oceans absorbing a quarter of anthropogenic emissions[3–5]. Early simulations with physics-only models showed that the combined effects of warming, changes in circulation and sea ice cover lead to reduced anthropogenic CO_2 uptake and thus decreased ocean carbon storage[6–9], amplifying climate change[10]. Including biology leads to a smaller decrease due to an accumulation of natural regenerated carbon at depth, which compensates for the decrease in anthropogenic CO_2 uptake. The balance between the two has, however, been much debated[7,11] as these changes impact both the natural carbon cycle and the ocean uptake of anthropogenic carbon, which complicates the response.

More recent analysis of model simulations[12] performed as part of the Coupled Model Intercomparison Project (CMIP)[13] have generally corroborated these results, although the effects of circulation, warming and sea ice could not be separated and simulated changes were ascribed almost entirely to circulation. In these models, surface buoyancy input reduces deep water formation and Meridional Overturning Circulation (MOC) in both the Atlantic (AMOC) and Southern Ocean and increases regenerated carbon[12,14], albeit with the important caveat that C_{reg} was estimated using the apparent oxygen utilization (AOU) approximation (Methods). In addition to

[1]School of International Liberal Studies, Waseda University, Tokyo, Japan. [2]Independent Researcher, London, UK. [3]College of Earth, Ocean and Atmospheric Sciences, Oregon State University, Corvallis, OR, USA. ✉e-mail: samar.khatiwala@waseda.jp

https://doi.org/10.1038/s41558-026-02686-x

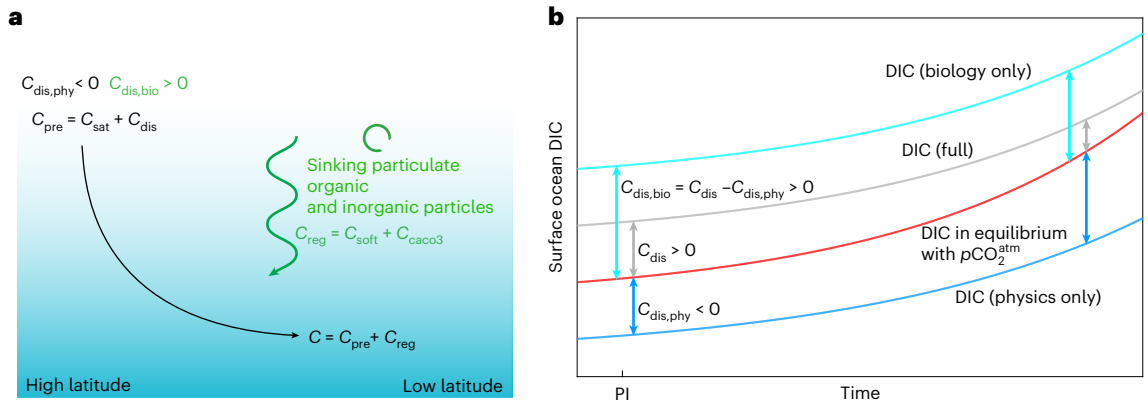

Fig. 1 | Preformed, regenerated and disequilibrium carbon. a, Schematic illustrating carbon decomposition. The surface concentration of any tracer is known as its preformed value[61]. Propagating this (space- and time-varying) field conservatively into the interior by ocean circulation gives the three-dimension distribution of the corresponding preformed tracer. For DIC, its surface value C_{pre} can be decomposed into a component C_{sat} in solubility equilibrium, with the atmosphere and a residual C_{dis} representing disequilibrium, and these further into physical and biological contributions, $C_{sat} = C_{sat,phy} + C_{sat,bio}$ and $C_{dis} = C_{dis,phy} + C_{dis,bio}$. DIC produced from remineralization and dissolution of particulate organic and inorganic carbon gives rise to regenerated carbon (C_{reg}). The interior DIC concentration (C) is the sum of C_{pre} and C_{reg}. Adapted from ref. 18. **b**, Schematic illustrating response of surface carbon disequilibrium components in high-latitude regions of ocean ventilation to rising pCO_2^{atm}. In the abiotic model, surface ocean DIC (lower blue line) is less than the DIC in equilibrium with the extant pCO_2^{atm} (red line) in the PI ($C_{dis,phy} < 0$) because upwelling waters in the Southern Ocean are relatively warm and lose heat to the atmosphere as they move south. This heat loss increases CO_2 solubility and leads to local ingassing of carbon from the atmosphere[22], which is incomplete due to slow air–sea exchange leaving waters undersaturated. $C_{dis,phy}$ grows over time as pCO_2^{atm} increases at a faster rate than the surface ocean, and its change $\Delta C_{dis,phy}$ is thus negative. Surface DIC in the full biotic model (grey line) is higher than equilibrium DIC ($C_{dis} > 0$) in the PI because biologically mediated disequilibrium ($C_{dis,bio}$; difference between the upper cyan and red lines) is positive due to upwelling and incomplete outgassing of respired carbon in the Southern Ocean, leading to supersaturation[23,38,41]. C_{dis} decreases over time so that the change ΔC_{dis} is negative. As described in Methods and Extended Data Fig. 2, because the equilibration time in the biotic model is less than in the abiotic model, ΔC_{dis} is more negative than $\Delta C_{dis,phy}$, and therefore $\Delta C_{dis,bio}$ (= $\Delta C_{dis} - \Delta C_{dis,phy}$) is also negative.

neglecting C_{caco3}, AOU has been shown to yield qualitatively incorrect estimates of C_{soft} (refs. 11,15–21). This directly affects C_{reg} estimates, and indirectly other components of DIC such as 'preformed' carbon (C_{pre}), which is often evaluated as the residual C_{pre} = DIC − C_{reg}. Preformed carbon is the DIC concentration resulting from propagation of surface values, which are set by both the solubility and biological pumps, into the ocean interior by circulation (Fig. 1). The decomposition DIC = C_{pre} + C_{reg} is central to understanding the ocean carbon cycle's response to climate change[12].

Past studies were based on concentration-driven simulations for which changes in ocean carbon storage cannot readily be converted to atmospheric CO_2 owing to buffer chemistry. In addition, buffering slows down equilibration of CO_2 (~1 year) with the atmosphere, resulting in surface waters that are frequently out of solubility equilibrium due to both physical ($C_{dis,phy}$) and biological ($C_{dis,bio}$) processes[22,23] (Fig. 1). This disequilibrium signal, which can be positive or negative depending on whether the surface water is over- or undersaturated with respect to solubility equilibrium with the atmosphere (C_{sat}), propagates into the ocean interior and affects carbon storage as part of preformed carbon, an aspect not previously considered in global warming scenarios. In the present-day ocean, $C_{dis,phy}$ is estimated to reduce carbon storage by 700–800 PgC, while $C_{dis,bio}$ increases it by 1,000–1,200 PgC (refs. 1,18,24). Moreover, it has been shown that disequilibrium components are crucial to understanding changes in carbon storage and pCO_2^{atm} under large climate shifts, such as under global warming[11] or from glacial to interglacial periods[18,25,26].

Here, we use an ocean biogeochemical model (Model of Ocean Biogeochemistry and Isotopes (MOBI)-transport matrix method (TMM))[18,27,28] driven by circulation and forcing fields from the University of Victoria Earth System Climate Model (UVic ESCM)[29,30] to investigate the effects of climate change on the different DIC components between 1765 and 2500 and their feedback on atmospheric CO_2 (Methods). Diagnostic tracers[18,24], which circumvent inaccuracies associated with the AOU approximation, and attribution experiments are used to robustly quantify the impact of different forcing mechanisms under a range of Shared Socioeconomic Pathway (SSP) emission scenarios[31,32], and thus better understand the multi-centennial consequences of anthropogenic carbon emissions on climate[33].

Climate change impacts on ocean physical state

The physical and biogeochemical response of the model to increasing pCO_2^{atm} (Fig. 2) include an increase in sea surface temperature (SST); decreases in AMOC and sea ice extent; and reductions in net primary production (NPP) and particulate organic carbon (POC) export (export production, EP). These changes are generally in line with the more complex ESM simulations in CMIP (Methods).

To investigate how changes in the ocean carbon cycle affect atmospheric CO_2, MOBI-TMM is coupled to a single-box atmosphere whose pCO_2^{atm} is prognostically time-stepped as a balance between imposed emissions (diagnosed for each SSP scenario) and the air–sea flux of CO_2 (Methods). Five transient experiments were performed for each scenario. In the first (labelled 'All'), time-varying circulation, temperature and sea ice concentration were specified. In the next experiment, these forcing fields were held at their preindustrial (PI) value. This 'No climate change' ('NCC') experiment allows separation of the (relatively small) impact of climate change on the marine carbon cycle from the (much larger) impact of rising atmospheric CO_2. In the final three experiments, we separately probe the impacts of changes in circulation ('Circulation'), warming ('Temperature') and reduced sea ice cover ('Sea ice'), by specifying time-varying fields of one of those forcing fields from the UVic ESCM simulation in turn, with the other two held fixed at their PI value.

For SSP5-8.5, in the absence of climate change, pCO_2^{atm} is lower by ~33 ppm in 2100 and by ~271 ppm in 2500 (Fig. 3a). When circulation and temperature are independently allowed to change, CO_2 levels in 2500 increase from their NCC value by 196 and 105 ppm, respectively. Sea ice has a negligible effect. These values quantify the feedback of ocean climate change on pCO_2^{atm}, which will in turn lead to further changes in climate. This additional effect is not accounted for in our offline simulations but is estimated to be quite small (Methods).

https://doi.org/10.1038/s41558-026-02686-x

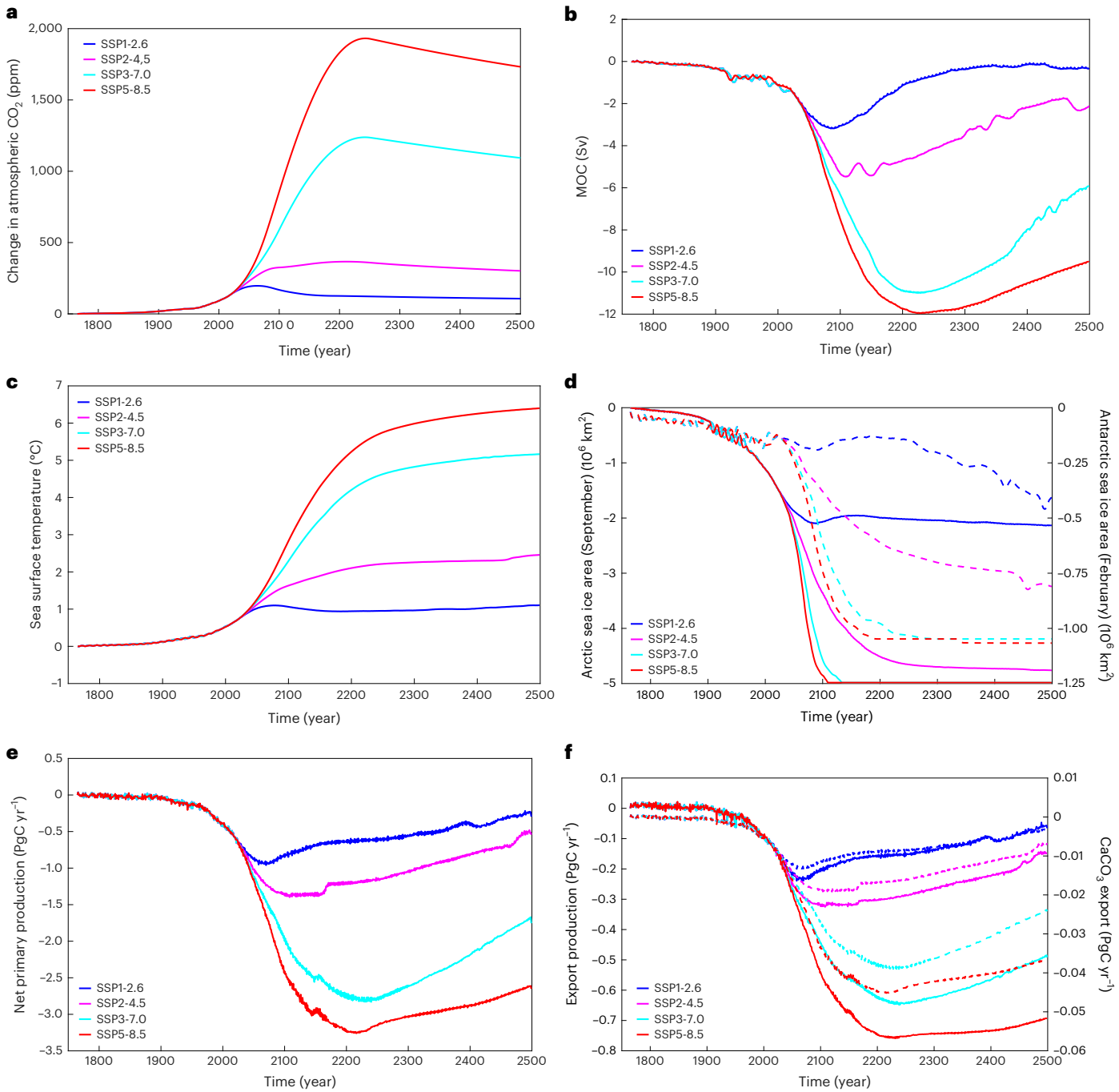

Fig. 2 | Simulated changes in ocean physical and biogeochemical variables. **a**, Prescribed atmospheric CO_2 for the SSP1-2.6, SSP2-4.5, SSP3-7.0 and SSP5-8.5 emission scenarios used to force the UVic ESCM model between 1765 and 2500. **b**–**f**, Simulated change from PI in AMOC (**b**), global mean SST (**c**), Arctic (solid lines, left axis) and Antarctic (dashed lines, right axis) sea ice area (**d**), NPP (**e**), and POC export (solid lines, left axis) and $CaCO_3$ export (dashed lines, right axis) (**f**) for each scenario.

In our closed-system simulations, differences in pCO_2^{atm} with and without climate change can only arise from changes in marine carbon storage. To better understand this, we partition total DIC $C = C_{sat,phy} + C_{sat,bio} + C_{dis,phy} + C_{dis,bio} + C_{soft} + C_{caco3}$ (ref. 18; see above, Fig. 1 and Methods).

Response of carbon components to rising atmospheric CO_2

The carbon decomposition for the PI run (Fig. 3b and Supplementary Table 1) yields values close to estimates from a data-constrained model[1,21], with subsequent changes in response to anthropogenic emissions dominated by the uptake of CO_2 due to rising atmospheric CO_2 concentrations. Before considering the impact of climate change, we therefore remove this 'baseline' signal as simulated by the NCC experiment. In this experiment, for SSP5-8.5, $C_{sat,phy}$ shows the largest increase (Fig. 3c; see Extended Data Fig. 1 for other scenarios). The disequilibrium components also undergo large changes as the surface ocean lags the growth in pCO_2^{atm} due to buffering (Fig. 1b), with $C_{dis,phy}$ becoming more negative and $C_{dis,bio}$ less positive over time (Fig. 1b, Extended Data Fig. 2 and Methods), overall reducing ocean carbon storage in year 2500 by ~305 PgC relative to solubility equilibrium. There is little to no change in C_{soft} and C_{caco3}. In the following, these

https://doi.org/10.1038/s41558-026-02686-x

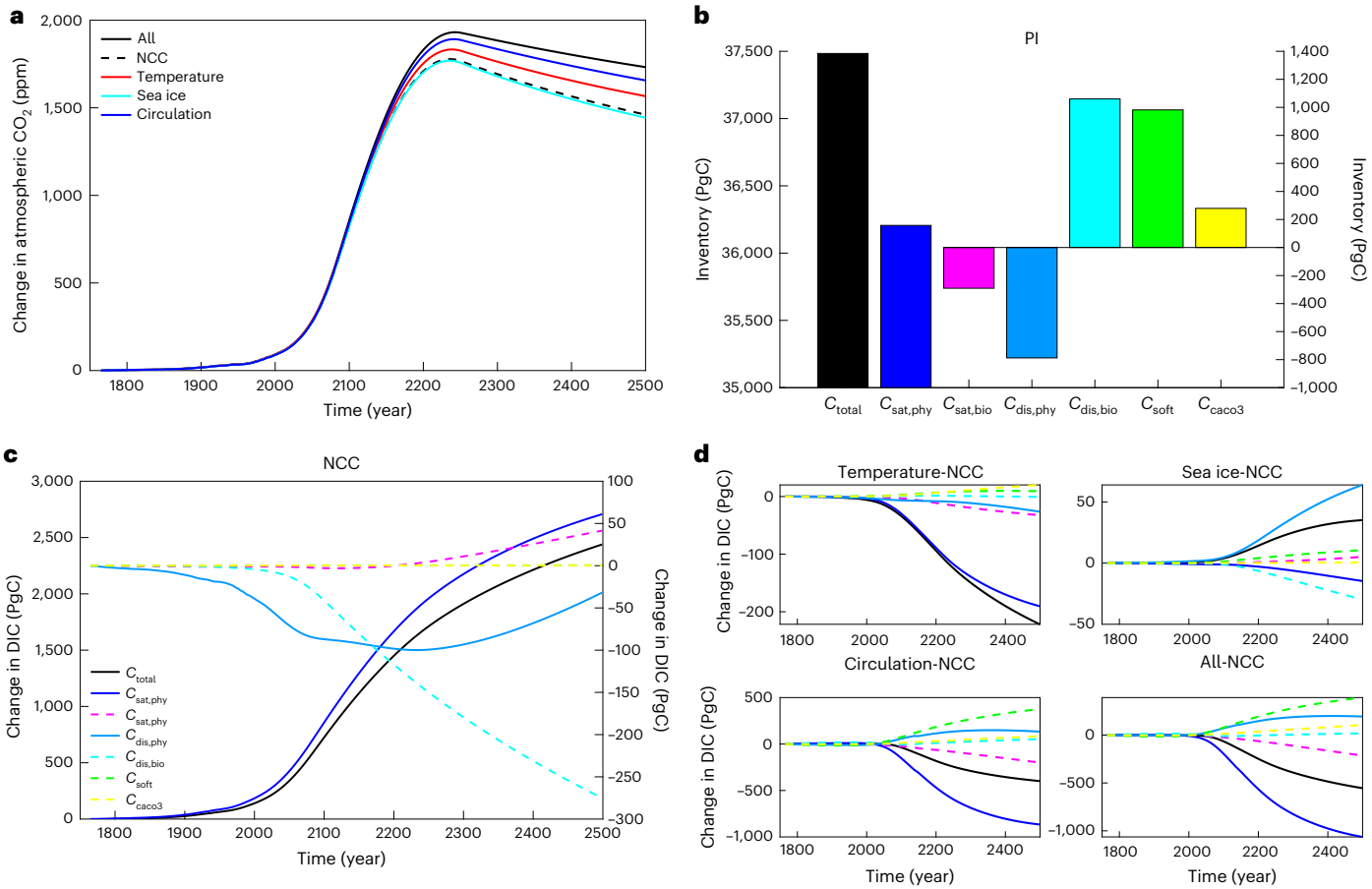

Fig. 3 | Evolution of marine carbon components under global warming. **a**, Change in atmospheric CO_2 in emission-driven simulations with and without climate change for the SSP5-8.5 scenario. **b**, Carbon components in the PI. **c**, Changes in carbon components in the NCC simulation. Left axes in **b** and **c** apply to C_{total} and $C_{sat,phy}$, and right axes to the other components. All components sum up to C_{total}. In **c**, the curve for C_{soft} is hidden under that for C_{caco3}. **d**, Changes in carbon components with respect to NCC in response to different forcing factors for SSP5-8.5 (see **c** for the legend). See Extended Data Fig. 1 for corresponding plots for other scenarios.

changes in the NCC experiment are subtracted from each attribution experiment to isolate the climate change signal.

Impact of climate change on carbon components

In the Circulation experiment, under SSP5-8.5 there is a large decrease in $C_{sat,phy}$ as transport of anthropogenic carbon from high-latitude ventilation regions into the interior is suppressed (Figs. 3d and 4a, and Supplementary Table 1; see Extended Data Figs. 1 and 3 for other scenarios). This is the primary cause of the ~900 PgC decrease by 2500 in C_{pre}, more than half of which is compensated by an increase in C_{reg} (Fig. 4e and Extended Data Table 1) as a slower circulation allows more time (quantified by an increase in ventilation age) (Methods and Extended Data Fig. 4) for its accumulation[9,11,12]. This is despite large decreases in NPP and EP (Extended Data Fig. 5), which we attribute to reduced nutrient upwelling[12,34–37]. Under SSP1-2.6 (Fig. 4b), there is a similar decrease in C_{pre} and increase in C_{reg}. However, in contrast to the high-emission case, the change in C_{pre} is primarily due to $C_{sat,bio}$ and the compensation is nearly exact (Fig. 4e), leading to no net change, despite large changes in individual components.

A slower circulation also allows surface waters to equilibrate more, enhancing carbon storage. Initially, biological disequilibrium (and, thus, storage) decreases, but as C_{reg} builds up in the ocean interior, $C_{dis,bio}$ increases, amplifying biological carbon storage[18,38]. $C_{dis,phy}$ and $C_{dis,bio}$ together increase storage by ~41% more than by C_{reg} alone under SSP5-8.5 (Supplementary Table 1).

Circulation also has a surprisingly large impact on the biological saturation term, $C_{sat,bio}$. Sinking $CaCO_3$ transfers alkalinity from the surface to the deep ocean, decreasing CO_2 solubility[39], an effect quantified by $C_{sat,bio}$, which is −290 PgC in our PI simulation. A slowing circulation enhances accumulation of regenerated alkalinity in the deep ocean (Fig. 5a and Supplementary Fig. 4), decreasing $C_{sat,bio}$ even further[40]. This effect is proportionately larger under low emissions (Fig. 4b and Extended Data Fig. 3). Accounting for changes in $C_{sat,bio}$ due to differences in pCO_2^{atm} between the various experiments (Methods), we estimate that roughly half the change in $C_{sat,bio}$ (~100 PgC in SSP5-8.5) is caused by redistribution of alkalinity.

In the Temperature experiment, the direct effect of warming is to decrease CO_2 solubility and, hence, $C_{sat,phy}$. This is the largest contributor to the decrease in C_{pre} under high emissions (Fig. 4c and Extended Data Fig. 3). By contrast, under low emissions (Fig. 4d), $C_{dis,phy}$ makes up the dominant component of the reduction in C_{pre}. The reason $C_{dis,phy}$ decreases in a warmer ocean is that the meridional SST gradient in the Southern Ocean increases as the polar ocean remains close to the freezing point whereas the subpolar ocean warms substantially (Extended Data Fig. 6). This increases the magnitude of the (negative) physical disequilibrium and thus decreases ocean carbon storage. This effect is proportionately larger under low emissions than the solubility-driven decline in $C_{sat,phy}$ (Supplementary Table 1).

Warming also promotes phytoplankton growth, zooplankton grazing and remineralization[28], giving rise to an increase in NPP and EP (Extended Data Fig. 5). The resulting increase in C_{reg} is, however, too small under any of the scenarios to compensate for the decline in C_{pre} (Fig. 4e). For SSP5-8.5, the overall change in biological carbon storage

https://doi.org/10.1038/s41558-026-02686-x

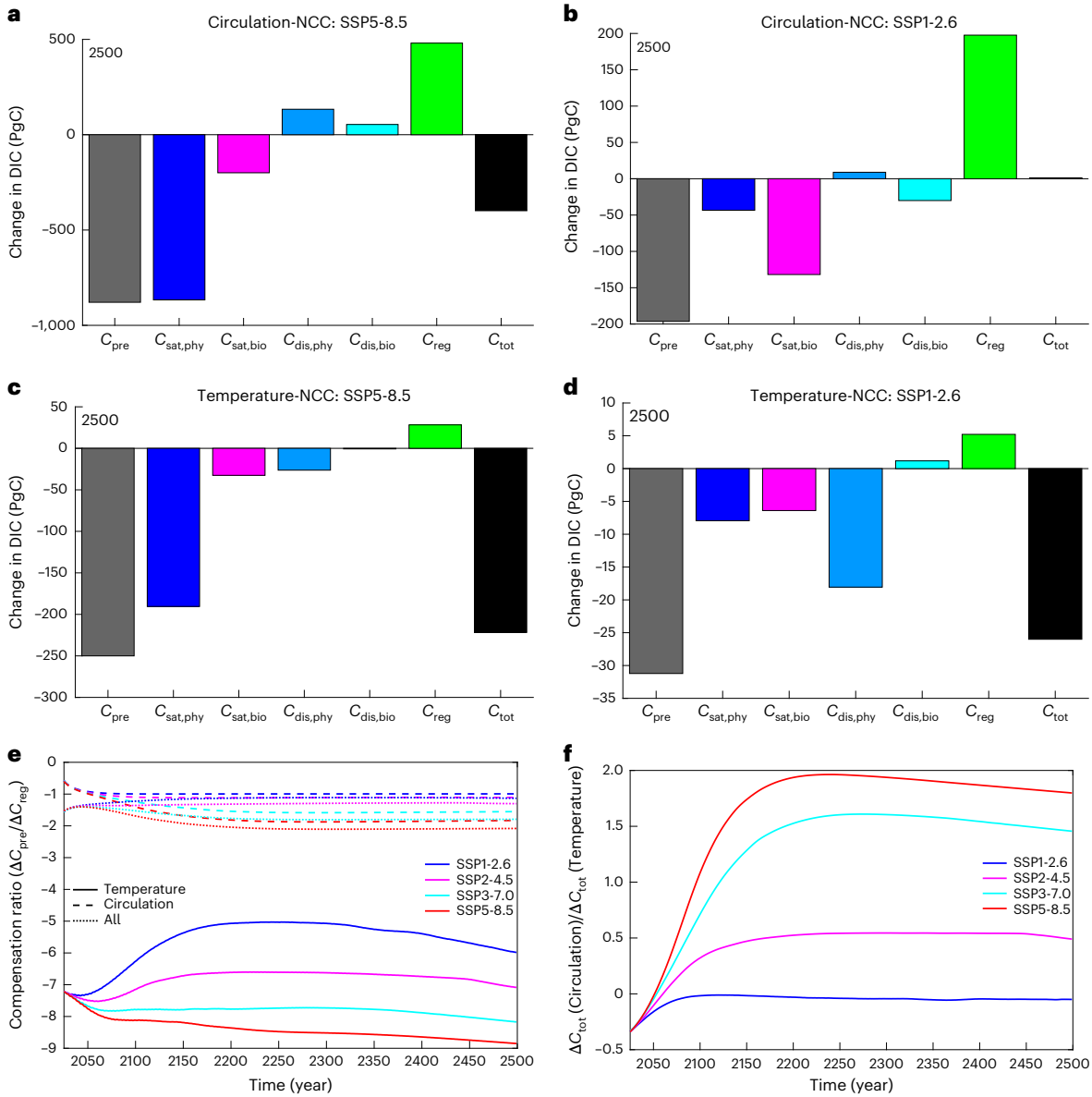

Fig. 4 | Impact of circulation and warming on carbon components. a,**b**, Change in carbon components with respect to NCC in year 2500 due to circulation under SSP5-8.5 (**a**) and SSP1-2.6 (**b**). **c**,**d**, Change in carbon components due to warming under SSP5-8.5 (**c**) and SSP1-2.6 (**d**). **e**, Compensation ratio of change (Δ) in preformed to regenerated carbon with respect to NCC in the Temperature (solid lines), Circulation (dashed lines) and All (dotted lines) attribution experiments for the four emission scenarios as a function of time. **f**, Ratio of change in total carbon storage in the Circulation attribution experiment to that in the Temperature experiment for the four emission scenarios as a function of time.

(sum of $C_{sat,bio} + C_{dis,bio} + C_{reg}$) is close to zero, confirming the results of previous studies that neither NPP nor EP are robust indicators of biological carbon storage[12,41–44].

Lastly, the primary effect of reduced sea ice cover is to facilitate gas exchange, making $C_{dis,phy}$ less negative and $C_{dis,bio}$ less positive[11] (Extended Data Fig. 7 and Supplementary Table 1). The former change generally outweighs the latter, leading to an overall increase in storage. However, for all scenarios, sea ice has a much smaller effect than temperature and circulation.

When all climate change factors are simultaneously applied, total carbon storage decreases by between 27 PgC and 554 PgC for the lowest and highest emissions, respectively (Supplementary Table 1). This response is surprisingly linear in SSP5-8.5, that is, the values are close to the sum of the change in storage for individual factors, with the deviation from linearity less than 2% in 2100 and still under 6% in 2500.

Evaluation of the AOU approximation of C_{soft}

These results rely on separate, explicit simulations of diagnostic tracers to accurately partition DIC into its components (Methods). When these are not available, as in most CMIP models and studies based on them[12,14,45,46], the partitioning is typically based on estimating C_{soft} via AOU (Methods), leading to substantial biases[11,15–21]. In our PI simulation, AOU overestimates true C_{soft} by ~45%, versus ~34% in a data-constrained model[1,21]. In the transient SSP5-8.5 simulations, in both the Temperature and Sea ice experiments, there is an increase in C_{soft} but AOU indicates a decrease (Methods, Extended Data Fig. 8 and Supplementary Table 2). This is consistent with other studies showing that AOU can give qualitatively incorrect estimates of C_{soft} change when large climatic shifts are involved[19]. For the Circulation experiment, AOU is reasonably accurate, slightly overestimating (underestimating) the true change in C_{soft} (C_{reg}) by ~10% (~14%). However, when all three climate change factors are combined, AOU underestimates C_{soft} and C_{reg} changes by ~31% and ~47%,

https://doi.org/10.1038/s41558-026-02686-x

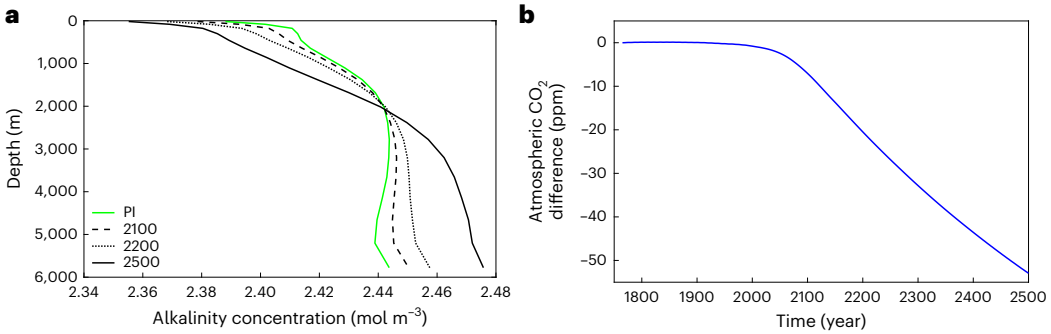

Fig. 5 | Circulation-driven redistribution of alkalinity. a, Global mean profiles of alkalinity in the PI and years 2100, 2200 and 2500 for the SSP5-8.5 scenario showing the increasing accumulation of alkalinity in the deep ocean under global warming, and a corresponding decrease at the surface. **b**, Difference in atmospheric CO_2 between the Circulation experiment with surface alkalinity held fixed at its PI value and the standard Circulation experiment (Methods). Higher surface alkalinity in the former leads to greater uptake of anthropogenic carbon and, hence, a lower atmospheric CO_2.

respectively. These errors are comparable to, and in some cases larger than, the signals of interest, highlighting the need for caution when interpreting AOU-based estimates of carbon storage[11,15–19], especially under climate change.

Feedback on atmospheric CO_2

Our emission-driven simulations allow the direct mapping of changes in the carbon components to pCO_2^{atm} changes for each attribution experiment by scaling the total change in pCO_2^{atm} by the fractional contribution of a component to the total change in DIC. The increase in pCO_2^{atm} due to reduced ocean carbon storage because of climate change ranges from ~16 ppm for SSP1-2.6 to ~271 ppm for SSP5-8.5 in 2500 (Fig. 6, Extended Data Fig. 9 and Supplementary Table 1). The largest contributing factor for high emissions is the effect of circulation on $C_{sat,phy}$, which raises pCO_2^{atm} in 2500 by more than 400 ppm for SSP5-8.5, more than half of which is balanced by C_{reg}. $C_{dis,phy}$ also decreases; this previously overlooked effect on C_{pre}, which for SSP5-8.5 produces ~30% additional lowering in pCO_2^{atm} than by C_{reg} alone, has also been shown to be relevant for lowering atmospheric CO_2 during other periods of weak overturning, such as the Last Glacial Maximum (LGM)[18].

For low-emission scenarios, the direct effects of temperature become dominant (Fig. 4f). This is because of warming effects on $C_{dis,phy}$, which makes a relatively large contribution to the decrease in preformed carbon for those scenarios (60% and 31%, respectively, for SSP1-2.6 and SSP2-4.5; Supplementary Table 1). This amplifies the (negative) physical disequilibrium and thus decreases carbon storage. In SSP1-2.6 for instance, 75% of the total increase in pCO_2^{atm} in year 2500 in the Temperature experiment is caused by $C_{dis,phy}$. A similar effect, but of opposite sign, has been seen in simulations of the LGM[18].

$C_{sat,bio}$ in the SSP5-8.5 circulation experiment increases pCO_2^{atm} in 2500 by ~94 ppm, of which we estimate ~53 ppm is due to increasing sequestration of alkalinity in the deep ocean (Methods). The effect of circulation changes on $C_{sat,bio}$ becomes even more important relative to the other components at lower emissions. For example, in SSP1-2.6 it contributes to an increase in pCO_2^{atm} of ~30 ppm, offsetting nearly all the decrease due to C_{soft} (Supplementary Table 1). Although this reinforcing feedback on climate has been previously recognized[40], its magnitude has, to our knowledge, not been quantified.

Discussion

In this study, we have quantified the impact of global warming on marine carbon storage components and the consequent feedbacks on atmospheric CO_2 due to different forcing factors and for a range of emission scenarios. This has proven difficult in the past, both because of the complex responses of the various carbon components to climate change and because conventional models, such as those used in CMIP, are typically not equipped with the diagnostic tracers required to robustly quantify these components. Moreover, translating changes in storage to changes in atmospheric CO_2 is not straightforward in concentration-driven CMIP simulations because of buffering.

Consistent with previous work[7–9,12], we find that increased regenerated carbon under climate change offsets reduced anthropogenic carbon uptake. However, while previous studies have attributed this compensation between C_{pre} and C_{reg}, explicitly or implicitly, almost entirely to a slowing circulation[12,14], our results instead show that the degree of compensation depends on the forcing factor and emission scenario. Across all scenarios, circulation does indeed elicit the largest response relative to other forcing factors (Fig. 4 and Extended Data Figs. 3 and 7), with the changes tending to compensate each other[12] (Fig. 4e). However, we additionally find that the degree of compensation ranges from almost exact for SSP1-2.6 to about half for SSP5-8.5 (Fig. 4e).

Moreover, while the direct effects of warming induce smaller changes, they are far less balanced as the decrease in preformed carbon is much greater than the increase in regenerated carbon from higher primary production, export and remineralization (Fig. 4e). Consequently, warming dominates the overall response at lower emissions and continues to contribute substantially at higher emissions (Fig. 4f). Interestingly, for all scenarios, the degree of compensation and the relative contributions of warming and circulation are, after an initial adjustment, relatively stable over time (Fig. 4f).

Mapped to atmospheric CO_2, global warming-driven changes in ocean circulation, temperature and sea ice under SSP5-8.5 raise pCO_2^{atm} by 271 ppm (~16%) by 2500 (Fig. 6d, All) relative to a simulation without such changes. A slowdown in the overturning circulation both reduces anthropogenic carbon uptake and increases accumulation of alkalinity at depth, increasing pCO_2^{atm} by ~425 ppm (Fig. 6d, Circulation) and ~53 ppm (Fig. 5b), respectively. Concomitantly, it allows for greater sequestration of regenerated carbon[11,12] and reduced physical air–sea disequilibrium (Fig. 6d, Circulation), lowering pCO_2^{atm} by ~226 and 65 ppm, respectively.

Under high mitigation and stabilization scenarios, warming dominates, contributing to nearly all of the ~16 ppm increase in pCO_2^{atm} for SSP1-2.6 (Fig. 6b, Temperature). Even for SSP5-8.5, warming still contributes to a third (~105 ppm) of the total increase (Fig. 6d, Temperature).

The simulations also identify the first-order role of air–sea disequilibrium in modulating carbon storage under climate change. Disequilibrium has been shown to be key to explaining lower atmospheric CO_2 during glacial periods[18,25,26]. Under global warming, as in the LGM[18], a slower circulation enhances carbon uptake by reducing physical disequilibrium; for SSP5-8.5, this amplifies by 30% the impact of C_{reg} alone on lowering pCO_2^{atm}. Meanwhile, warming enhances physical disequilibrium because of an increase in the meridional SST gradient (Extended Data Fig. 6), reducing storage. A similar effect but of

https://doi.org/10.1038/s41558-026-02686-x

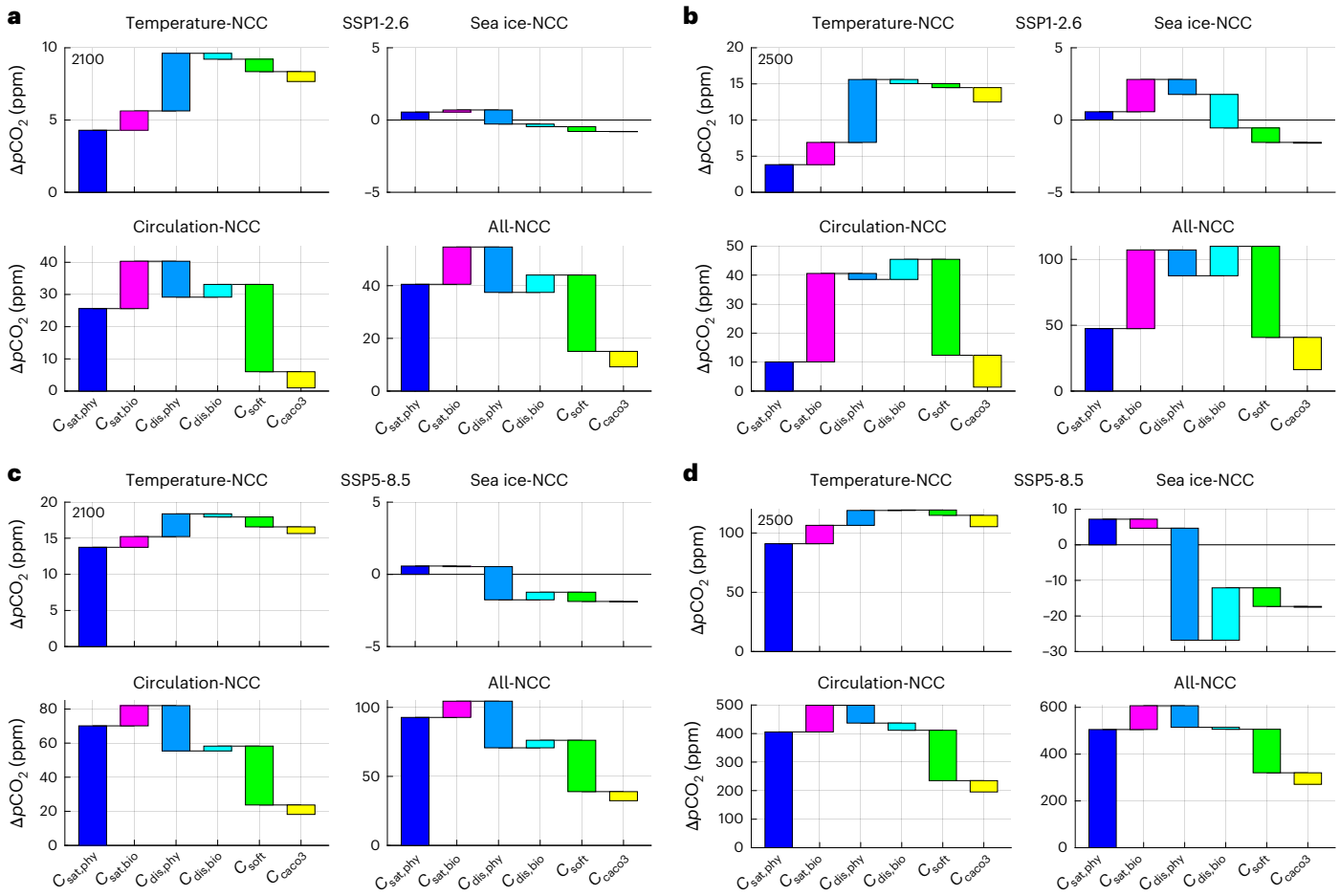

Fig. 6 | Impact of marine carbon pumps on atmospheric CO_2. a–d, Waterfall chart attributing changes in atmospheric CO_2 to different carbon components and forcing factors in years 2100 (**a** and **c**) and 2500 (**b** and **d**) for the lowest SSP1-2.6 (**a** and **b**) and highest SSP5-8.5 (**c** and **d**) emission scenarios. Each bar represents a component with its height corresponding to the (positive or negative) change in pCO_2^{atm} due to that component. From left to right, each panel for a particular forcing factor shows the cumulative change in pCO_2^{atm} as successive components are included. See Extended Data Fig. 9 for equivalent plots for the SSP2-4.5 and SSP3-7.0 scenarios.

opposite sign has been simulated for the LGM and shown to nearly double the solubility-driven drawdown of CO_2 during that period[18]. This effect is especially pronounced under low and intermediate emissions and explains the dominance of temperature over circulation under those scenarios.

Our results underscore the importance of accurately diagnosing marine carbon components in models. Estimates of C_{reg} based on AOU can have errors ranging from 50% to over 1,000%, depending on the forcing factor and emissions scenario, with even the direction of change sometimes predicted incorrectly (Extended Data Fig. 8 and Supplementary Table 2). The large resulting errors in the attribution of simulated carbon cycle changes to different forcing factors and processes[12,14] could be especially relevant in the context of achieving net zero emissions and efforts to sequester CO_2 in the deep ocean through marine carbon dioxide removal strategies[47,48].

Although the large-scale metrics of ocean physical and biogeochemical change projected by UVic ESCM-MOBI are within the spread of CMIP models[12,34], our study has several limitations. First, it is based on a single realization of UVic ESCM, an intermediate-complexity climate model. Second, in the configuration employed here, UVic ESCM does not account for climate-induced changes in winds (Methods), which may affect both the simulated warming (for example, amplifying it[49]) and the resulting carbon cycle response (for example, enhancing outgassing of natural carbon[50,51]). Third, in common with many biogeochemical models in CMIP, MOBI neglects the impact of acidification on the formation and dissolution of $CaCO_3$ (ref. 52); assumes a fixed stoichiometry for organic matter; simulates only a small number of plankton types; and parameterizes the sinking and remineralization of POC in a simplistic way that likely does not resolve spatial variations in its transfer efficiency to depth. These aspects are recognized to be important for the marine carbon cycle and its potential response to climate change[53] but remain poorly constrained even for the present-day ocean[54,55]. Lastly, our simulations did not include a terrestrial carbon cycle component. This may affect our attribution experiments as some of the carbon outgassed by the ocean could be absorbed by land, moderating the atmospheric response[56]. Given these caveats and the persistent, large uncertainties in projected changes in the ocean carbon cycle[12,14,34,53,57–60] and its potential feedbacks on climate, it is imperative that a similar analysis be conducted with a wider group of models instrumented with the appropriate diagnostic tracers to robustly quantify changes in marine carbon components. Such an exercise would enhance understanding of and better constrain the complex marine carbon cycle response to climate change.

Online content

Any methods, additional references, Nature Portfolio reporting summaries, source data, extended data, supplementary information, acknowledgements, peer review information; details of author contributions and competing interests; and statements of data and code availability are available at https://doi.org/10.1038/s41558-026-02686-x.

References

1. DeVries, T. The ocean carbon cycle. *Annu. Rev. Environ. Resour.* **47**, 317–341 (2022).
2. Volk, T. & Hoffert, M. I. in *The Carbon Cycle and Atmospheric CO_2: Natural Variations Archean to Present* (eds Sundquist, E. T. & Broecker, W. S.) 99–110 (American Geophysical Union, 1985); https://doi.org/10.1029/GM032p0099
3. Khatiwala, S., Primeau, F. & Hall, T. Reconstruction of the history of anthropogenic CO_2 concentrations in the ocean. *Nature* **462**, 346–349 (2009).
4. DeVries, T. & Primeau, F. Dynamically and observationally constrained estimates of water-mass distributions and ages in the global ocean. *J. Phys. Oceanogr.* **41**, 2381–2401 (2011).
5. Friedlingstein, P. et al. Global carbon budget 2023. *Earth Syst. Sci. Data* **15**, 5301–5369 (2023).
6. Joos, F., Plattner, G.-K., Stocker, T. F., Marchal, O. & Schmittner, A. Global warming and marine carbon cycle feedbacks on future atmospheric CO_2. *Science* **284**, 464–467 (1999).
7. Matear, R. J. & Hirst, A. C. Climate change feedback on the future oceanic CO_2 uptake. *Tellus B* **51**, 722–733 (1999).
8. Sarmiento, J. L., Hughes, T. M. C., Stouffer, R. J. & Manabe, S. Simulated response of the ocean carbon cycle to anthropogenic climate warming. *Nature* **393**, 245–249 (1998).
9. Sarmiento, J. L. & Le Quéré, C. Oceanic carbon dioxide uptake in a model of century-scale global warming. *Science* **274**, 1346–1350 (1996).
10. Friedlingstein, P. et al. Positive feedback between future climate change and the carbon cycle. *Geophys. Res. Lett.* **28**, 1543–1546 (2001).
11. Bernardello, R. et al. Response of the ocean natural carbon storage to projected twenty-first-century climate change. *J. Clim.* **27**, 2033–2053 (2014).
12. Liu, Y., Moore, J. K., Primeau, F. & Wang, W. L. Reduced CO_2 uptake and growing nutrient sequestration from slowing overturning circulation. *Nat. Clim. Change* **13**, 83–90 (2023).
13. Eyring, V. et al. Overview of the Coupled Model Intercomparison Project Phase 6 (CMIP6) experimental design and organization. *Geosci. Model Dev.* **9**, 1937–1958 (2016).
14. Wilson, J. D. et al. The biological carbon pump in CMIP6 models: 21st century trends and uncertainties. *Proc. Natl Acad. Sci. USA* **119**, e2204369119 (2022).
15. Russell, J. L. & Dickson, A. G. Variability in oxygen and nutrients in South Pacific Antarctic Intermediate Water. *Glob. Biogeochem. Cycles* **17**, 1033 (2003).
16. Ito, T., Follows, M. J. & Boyle, E. A. Is AOU a good measure of respiration in the oceans? *Geophys. Res. Lett.* **31**, L17305 (2004).
17. Duteil, O. et al. A novel estimate of ocean oxygen utilisation points to a reduced rate of respiration in the ocean interior. *Biogeosciences* **10**, 7723–7738 (2013).
18. Khatiwala, S., Schmittner, A. & Muglia, J. Air–sea disequilibrium enhances ocean carbon storage during glacial periods. *Sci. Adv.* **5**, eaaw4981 (2019).
19. Cliff, E., Khatiwala, S. & Schmittner, A. Glacial deep ocean deoxygenation driven by biologically mediated air–sea disequilibrium. *Nat. Geosci.* **14**, 43–50 (2021).
20. Cassar, N., Nicholson, D., Khatiwala, S. & Cliff, E. Decomposing the oxygen signal in the ocean interior: beyond decomposing organic matter. *Geophys. Res. Lett.* **48**, e2021GL092621 (2021).
21. Carter, B. R. et al. Preformed properties for marine organic matter and carbonate mineral cycling quantification. *Glob. Biogeochem. Cycles* **35**, e2020GB006623 (2021).
22. Toggweiler, J. R., Gnanadesikan, A., Carson, S., Murnane, R. & Sarmiento, J. L. Representation of the carbon cycle in box models and GCMs: 1. Solubility pump. *Glob. Biogeochem. Cycles* **17**, 1026 (2003).
23. Toggweiler, J. R., Murnane, R., Carson, S., Gnanadesikan, A. & Sarmiento, J. L. Representation of the carbon cycle in box models and GCMs, 2, organic pump. *Glob. Biogeochem. Cycles* **17**, 1027 (2003).
24. Schmittner, A. & Fillman, N. J. Carbon and carbon-13 in the preindustrial and glacial ocean. *PLoS Clim* **3**, e0000434 (2024).
25. Eggleston, S. & Galbraith, E. D. The devil's in the disequilibrium: multi-component analysis of dissolved carbon and oxygen changes under a broad range of forcings in a general circulation model. *Biogeosciences* **15**, 3761–3777 (2018).
26. Ödalen, M., Nycander, J., Oliver, K. I. C., Brodeau, L. & Ridgwell, A. The influence of the ocean circulation state on ocean carbon storage and CO_2 drawdown potential in an Earth system model. *Biogeosciences* **15**, 1367–1393 (2018).
27. Khatiwala, S. A computational framework for simulation of biogeochemical tracers in the ocean. *Glob. Biogeochem. Cycles* **21**, GB3001 (2007).
28. Schmittner, A. & Somes, C. J. Complementary constraints from carbon (^{13}C) and nitrogen (^{15}N) isotopes on the glacial ocean's soft-tissue biological pump. *Paleoceanography* **31**, 669–693 (2016).
29. Weaver, A. J. et al. The UVic earth system climate model: model description, climatology, and applications to past, present and future climates. *Atmos. Ocean* **39**, 361–428 (2001).
30. Mengis, N. et al. Evaluation of the University of Victoria Earth System Climate Model version 2.10 (UVic ESCM 2.10). *Geosci. Model Dev.* **13**, 4183–4204 (2020).
31. O'Neill, B. C. et al. The roads ahead: narratives for shared socioeconomic pathways describing world futures in the 21st century. *Glob. Environ. Change* **42**, 169–180 (2017).
32. Meinshausen, M. et al. The Shared Socio-economic Pathway (SSP) greenhouse gas concentrations and their extensions to 2500. *Geosci. Model Dev.* **13**, 3571–3605 (2020).
33. Clark, P. U. et al. Consequences of twenty-first-century policy for multi-millennial climate and sea-level change. *Nat. Clim. Change* **6**, 360–369 (2016).
34. Kwiatkowski, L. et al. Twenty-first century ocean warming, acidification, deoxygenation, and upper-ocean nutrient and primary production decline from CMIP6 model projections. *Biogeosciences* **17**, 3439–3470 (2020).
35. Moore, J. K. et al. Sustained climate warming drives declining marine biological productivity. *Science* **359**, 1139–1143 (2018).
36. Cabré, A., Marinov, I. & Leung, S. Consistent global responses of marine ecosystems to future climate change across the IPCC AR5 earth system models. *Clim. Dyn.* **45**, 1253–1280 (2015).
37. Bopp, L. et al. Multiple stressors of ocean ecosystems in the 21st century: projections with CMIP5 models. *Biogeosciences* **10**, 6225–6245 (2013).
38. Ito, T. & Follows, M. J. Air-sea disequilibrium of carbon dioxide enhances the biological carbon sequestration in the Southern Ocean. *Glob. Biogeochem. Cycles* **27**, 1129–1138 (2013).
39. Zeebe, R. & Wolf-Gladrow, D. *CO_2 in Seawater: Equilibrium, Kinetics, Isotopes* Vol. 65 (Elsevier, 2001).
40. Chikamoto, M. O., DiNezio, P. & Lovenduski, N. Long-term slowdown of ocean carbon uptake by alkalinity dynamics. *Geophys. Res. Lett.* **50**, e2022GL101954 (2023).
41. Marinov, I. et al. Impact of oceanic circulation on biological carbon storage in the ocean and atmospheric pCO_2. *Glob. Biogeochem. Cycles* **22**, GB3007 (2008).
42. Gnanadesikan, A. & Marinov, I. Export is not enough: nutrient cycling and carbon sequestration. *Mar. Ecol. Prog. Ser.* **364**, 289–294 (2008).
43. Koeve, W., Kähler, P. & Oschlies, A. Does export production measure transient changes of the biological carbon pump's feedback to the atmosphere under global warming? *Geophys. Res. Lett.* **47**, e2020GL089928 (2020).

44. Frenger, I. et al. Misconceptions of the marine biological carbon pump in a changing climate: thinking outside the "export" box. *Glob. Chang. Biol.* **30**, e17124 (2024).
45. Oka, A. Ocean carbon pump decomposition and its application to CMIP5 earth system model simulations. *Prog. Earth Planet. Sci.* **7**, 25 (2020).
46. Katavouta, A. & Williams, R. G. Ocean carbon cycle feedbacks in CMIP6 models: contributions from different basins. *Biogeosciences* **18**, 3189–3218 (2021).
47. Siegel, D. A., DeVries, T., Doney, S. C. & Bell, T. Assessing the sequestration time scales of some ocean-based carbon dioxide reduction strategies. *Environ. Res. Lett.* **16**, 104003 (2021).
48. National Academies of Science Engineering and Medicine *A Research Strategy for Ocean-Based Carbon Dioxide Removal and Sequestration* (National Academies Press, 2022); https://doi.org/10.17226/26278
49. McMonigal, K., Larson, S., Hu, S. & Kramer, R. Historical changes in wind-driven ocean circulation can accelerate global warming. *Geophys. Res. Lett.* **50**, e2023GL102846 (2023).
50. Le Quéré, C. et al. Saturation of the Southern Ocean CO_2 sink due to recent climate change. *Science* **316**, 1735–1738 (2007).
51. Bunsen, F., Nissen, C. & Hauck, J. The impact of recent climate change on the global ocean carbon sink. *Geophys. Res. Lett.* **51**, e2023GL107030 (2024).
52. Planchat, A., Bopp, L., Kwiatkowski, L. & Torres, O. The carbonate pump feedback on alkalinity and the carbon cycle in the 21st century and beyond. *Earth Syst. Dyn.* **15**, 565–588 (2024).
53. Henson, S. et al. Knowledge gaps in quantifying the climate change response of biological storage of carbon in the ocean. *Earths Future* **12**, e2023EF004375 (2024).
54. Rufas, A., Khatiwala, S., Bisson, K. M., Martin, A. P. & Bouman, H. A. Can we constrain geographical variability in the biological carbon pump's transfer efficiency from observations? *Geophys. Res. Lett.* **52**, e2024GL111203 (2025).
55. Doney, S. C. et al. Observational and numerical modeling constraints on the global ocean biological carbon pump. *Glob. Biogeochem. Cycles* **38**, e2024GB008156 (2024).
56. Tjiputra, J. F., Couespel, D. & Sanders, R. Marine ecosystem role in setting up preindustrial and future climate. *Nat. Commun.* **16**, 2206 (2025).
57. Rohr, T., Richardson, A. J., Lenton, A., Chamberlain, M. A. & Shadwick, E. H. Zooplankton grazing is the largest source of uncertainty for marine carbon cycling in CMIP6 models. *Commun. Earth Environ.* **4**, 212 (2023).
58. Rodgers, K. B. et al. Low-latitude mesopelagic nutrient recycling controls productivity and export. *Nature* **632**, 802–807 (2024).
59. Laufkötter, C. et al. Projected decreases in future marine export production: the role of the carbon flux through the upper ocean ecosystem. *Biogeosciences* **13**, 4023–4047 (2016).
60. Laufkötter, C. et al. Drivers and uncertainties of future global marine primary production in marine ecosystem models. *Biogeosciences* **12**, 6955–6984 (2015).
61. Sarmiento, J. L. & Gruber, N. *Ocean Biogeochemical Dynamics* (Princeton Univ. Press, 2006); https://doi.org/10.1515/9781400849079

Methods

Description of models and simulations

UVic ESCM. We simulate the impact of increasing atmospheric CO_2 on the ocean's physical state with the intermediate-complexity University of Victoria Earth System Climate Model (UVic ESCM)[29,30]. UVic ESCM is composed of a three-dimensional ocean general circulation model (1.8° × 3.6° × 19 layers) coupled to atmospheric energy–moisture balance, dynamic–thermodynamic sea-ice and land-surface components.

UVic ESCM was first integrated to a PI equilibrium with a fixed atmospheric CO_2 concentration (pCO_2^{atm}) of 277.44 ppm. The ocean circulation in the configuration has been extensively evaluated against hydrographic, CFC and radiocarbon data[62,63]. The model was then forced with historical and future scenarioMIP projections[31,64] of pCO_2^{atm} and aerosols[30,65] from 1765 to 2500 (Fig. 2) for four different SSP emission scenarios[31,32]: one low emission (SSP1-2.6), one intermediate (SSP2-4.5), one high (SSP3-7.0) and one very high emission (SSP5-8.5).

MOBI-TMM. The ocean carbon cycle is simulated with the Model of Ocean Biogeochemistry and Isotopes (MOBI)[28] coupled to the TMM[27] for offline simulation of biogeochemical tracers. MOBI is composed of three phytoplankton functional types, one zooplankton class, dissolved inorganic and organic carbon, dissolved oxygen (O_2) and alkalinity. Phytoplankton growth is limited by the macronutrients dissolved inorganic phosphorous (DIP) and nitrogen; the micronutrient iron, governed by a prognostic iron cycle driven by inputs from atmospheric dust, sediments and hydrothermal vents; and light. The latter is reduced in proportion to the fraction of a grid box covered with sea ice, which also similarly blocks air–sea fluxes of CO_2 and O_2. Primary production, respiration and zooplankton grazing rates are exponentially dependent on temperature. The sinking speed of POC increases linearly with depth. $CaCO_3$ production is tied to POC production via a constant rain ratio and is independent of the local saturation state. Dissolution is parameterized by assuming that the downward flux of $CaCO_3$ decreases exponentially with depth.

MOBI-TMM was first spun up to equilibrium with a fixed PI pCO_2^{atm} and seasonally repeating, monthly mean temperature, salinity, winds, sea ice and circulation (transport matrices, TMs) fields extracted from the UVic ESCM PI simulation. This was followed by a transient simulation from 1765 to 2500 for each SSP scenario driven by the corresponding pCO_2^{atm} and monthly mean, time-evolving TMs and other forcing fields from UVic ESCM (extracted for each month between 1765 and 2500[66]). The PI solution was constrained by a variety of biogeochemical and isotopic data and is extensively described elsewhere[62,63].

For the emission-driven simulations, MOBI-TMM is coupled to a single-box atmosphere whose CO_2 concentration is prognostically time-stepped as a balance between imposed emissions and the air–sea flux of CO_2. Effective emissions for each SSP scenario were diagnosed from the concentration-forced simulations as a difference between the instantaneous rate of change of pCO_2^{atm} and the air-to-sea flux of CO_2. By construction, the simulated pCO_2^{atm} obtained by forcing the emission-driven model with this diagnosed emission trajectory reproduces the original specified pCO_2^{atm}. These emissions include both sources incorporated into the scenario, such as fossil fuel combustion and land-use and land-cover change, as well as any potential response of the terrestrial biosphere, which is not included in our simulations.

Attribution experiments. To attribute changes in carbon storage to specific forcing factors, simulations with MOBI-TMM were carried out in which time-varying fields (for each emission scenario) of one factor were specified, while the others were held at their PI value. These experiments are labelled Temperature, Circulation and Sea ice. In two additional simulations, all three are either fixed at their PI value (NCC) or allowed to vary in time ('All'). By construction, the simulated atmospheric CO_2 in the All experiment reproduces the original prescribed CO_2 for that scenario. Attribution experiments such as these in which one forcing parameter is altered at a time require an offline scheme like the TMM. A conventional climate model would not allow such simulations.

Our study does not include either a land carbon or ocean sediment model, which may affect simulated changes in pCO_2^{atm}. For example, some of the CO_2 outgassed by the ocean in the attribution experiments could potentially be absorbed by land, moderating pCO_2^{atm} changes[56]. The effect of interactive sediments has been shown to be small on the timescales considered here[67].

Our study also excludes the impact of wind changes. In UVic ESCM, prescribed monthly climatological wind fields are used for advection of heat and moisture by the energy balance model, as well as for calculating air–sea fluxes of heat, moisture and momentum. Prognostically computed anomalies can be optionally added to the prescribed winds[29]. However, for consistency with the data-constrained PI configuration from which the transient simulations are initialized and in which this feedback was switched off[62,63], we did not utilize this capability in the transient runs either, which may affect the simulated response to emissions. Winds directly drive ocean circulation, which in turn can affect SST, warming patterns[68] and air–sea CO_2 flux[51] in a spatially and temporally heterogeneous manner. A recent study[49] estimated that changes to the wind-driven ocean circulation in recent decades have amplified global warming by 17%. However, on longer timescales, the buoyancy flux-driven decline in the AMOC, as simulated in our model, is likely to dominate and reduce surface warming[49,69,70]. Other studies[50,51] have shown that strengthened westerlies in the Southern Ocean promote outgassing of natural CO_2 via increased upwelling, thus reducing net CO_2 uptake. Meanwhile, intensified westerly winds and deeper mixed layers in the North Atlantic enhance CO_2 uptake[51]. Given this complexity and the fact that an intermediate-complexity model like UVic ESCM may struggle to simulate these different feedbacks, it is difficult to quantify the impact of neglecting wind changes on our results.

Comparison with CMIP models

Broadly, there is good agreement between our simulations (Fig. 2) and those from more complex CMIP Earth system models. In CMIP6 models, AMOC decreases by an average of 7.3 ± 2.7 Sv by 2100 under the highest-emission SSP5-8.5 scenario[12], compared with 7.4 Sv in UVic ESCM, while global mean SST increases by 3.5 ± 0.8 °C (ref. 34) and 2.8 °C, respectively. The change in sea ice area is more difficult to assess given the very large range simulated by CMIP6 models[71–73]. In these models, the Arctic reaches 'ice-free' conditions (defined as September sea ice area below 10^6 km^2) for the first time between 2014 and 2093 under SSP5-8.5, although the majority of models reach this state by 2050[71]. The corresponding year in our model is 2079. For the Antarctic, CMIP6 models simulate a loss of between 0 and 3.3×10^6 km^2 by 2100 in February under SSP5-8.5[73], compared with 0.75×10^6 km^2 in UVic ESCM.

There is also similarity in the impact of these physical changes on the ocean carbon cycle. For SSP5-8.5, MOBI-TMM projects decreases in NPP of 6.2% by 2100, POC export (EP) by 0.56 PgC yr^{-1} and biogenic $CaCO_3$ export by 7.2% (Fig. 2). While there is considerable variability amongst CMIP models in predicted NPP and $CaCO_3$ export, with uncertainty even in the sign of the change[34,52,58], these values are comparable to decreases of 3% ± 9% (ref. 34) and 1.1 ± 0.5 PgC yr^{-1} (ref. 12), respectively, in NPP and EP simulated by the CMIP6 ensemble, and a change in $CaCO_3$ export lying between −17.4% and +22.8% for the majority of models[52].

Decomposition of carbon storage

We decompose DIC into a 'preformed' component C_{pre} originating at the ocean surface and conservatively (that is, without any sources or sinks) advected and diffused by ocean circulation into the interior, and a regenerated component C_{reg} representing DIC produced by respiration of soft tissue organic matter (C_{soft}) and dissolution of $CaCO_3$ (C_{caco3}) in the interior and that has accumulated since the water was

last at the surface[61,74] (Fig. 1a). To accurately perform this decomposition, we simulate a suite of diagnostic preformed tracers (labelled with the subscript 'pre') by conservatively propagating MOBI-TMM's monthly mean surface fields of DIC, DIP and alkalinity (A_T) into the interior with TMs extracted from UVic ESCM. For the PI experiment, seasonally repeating surface fields are propagated with seasonally repeating, monthly mean TMs from the UVic PI configuration and the preformed tracers integrated to equilibrium. For the transient runs, preformed tracer fields are initialized from these equilibrium distributions, and corresponding time-evolving surface fields propagated with time-evolving, monthly mean TMs.

The regenerated components are calculated as

$$C_{\mathrm{soft}} = R_{\mathrm{C:P}}(\mathrm{DIP} - \mathrm{DIP}_{\mathrm{pre}})$$

$$C_{\mathrm{caco3}} = 0.5[A_{\mathrm{T}} - A_{\mathrm{T,pre}} + R_{\mathrm{N:P}}(\mathrm{DIP} - \mathrm{DIP}_{\mathrm{pre}})],$$

where $R_{C:P}$ and $R_{N:P}$ are constant stoichiometric ratios of carbon to phosphorus and nitrogen to phosphorus, respectively[61], in organic matter whose values ($R_{C:P} = 112$ and $R_{N:P} = 16$) are identical to those used in the model. A different version of MOBI with variable stoichiometry produces a carbon decomposition very similar to that in this study[24].

The impact of air–sea disequilibrium is quantified by further partitioning DIC at each surface grid point into a component C_{sat} in solubility equilibrium with the atmosphere and a residual C_{dis} representing disequilibrium. C_{sat} is calculated using the extant pCO_2^{atm} (fixed in the PI simulation and time-varying in the transient runs). C_{dis} can be either positive or negative depending on whether the DIC concentration is greater (oversaturated) or less (understaturated) than the corresponding solubility equilibrium value. C_{sat} and C_{dis} are conservatively propagated into the interior by the circulation. Integrated globally, C_{sat} represents the oceanic DIC inventory if the surface was in solubility equilibrium, and C_{dis} the enhancement or depletion relative to this hypothetical value due to disequilibrium. Note that pCO_2^{atm} evolves differently in each of our emission-driven attribution experiments, which affects C_{pre} and its partitioning into C_{sat} and C_{dis}. However, the carbon decomposition results are qualitatively very similar when the simulations are instead performed with a prescribed pCO_2^{atm} (Supplementary Note 1 and Supplementary Fig. 1).

Lastly, the various components are split into 'physical' and 'biological' ones (labelled with the subscript 'phy' and 'bio', respectively). For both the PI and each transient experiment, the physical components are computed by performing a parallel run of the model with the biological source/sink terms set to zero. The biological components are defined as the difference between the full model and physics-only model solutions. The PI physics-only run was forced with the same fixed pCO_2^{atm} as the full model. This choice of atmospheric boundary condition (BC) ensures that the physics-only simulations are driven by the same physical forcing fields (circulation, temperature, sea ice and so on) and the difference between the full and no-bio runs in both the PI and transient runs can be attributed to biological carbon and not contaminated by differences in physical forcing, which would make interpreting the results extremely difficult, if not impossible. We emphasize that this choice of BC for spinning up the physics-only PI experiment does not affect total saturation (C_{sat}) and disequilibrium (C_{dis}); it affects only how they are split between physical and biological contributions. Nor does it affect C_{soft} or C_{caco3}. It is also consistent with previous studies[1,11,22,23,38] and is the recommended protocol for abiotic simulations in CMIP[75]. The sensitivity of our results to this choice of BC is discussed in Supplementary Note 2 and Supplementary Fig. 2.

The decomposition of total DIC (C) is thus given by

$$\begin{aligned} C &= C_{\mathrm{pre}} + C_{\mathrm{reg}} = C_{\mathrm{sat}} + C_{\mathrm{dis}} + C_{\mathrm{reg}} \\ &= C_{\mathrm{sat,phy}} + C_{\mathrm{sat,bio}} + C_{\mathrm{dis,phy}} + C_{\mathrm{dis,bio}} + C_{\mathrm{soft}} + C_{\mathrm{caco3}}. \end{aligned}$$

$C_{sat,bio}$ is the biological contribution to equilibrium carbon. Formation of calcium carbonate shells removes alkalinity from the surface ocean, which lowers the equilibrium concentration of DIC from the value it would have in the absence of biology. $C_{sat,bio}$ is thus generally negative. In the PI simulation, $C_{sat,bio} = -292$ PgC, compared with $C_{sat,phy} = 36{,}209$ PgC.

This partitioning is performed at every model grid point and integrated globally to obtain the inventory of each component (C_{XX} denotes both concentration and inventory, with the meaning usually clear from the context).

Feedback from reduced ocean carbon storage due to climate change

Our attribution experiments use forcing fields from UVic ESCM driven by prescribed atmospheric CO_2 for the various SSP scenarios. However, by switching different forcing factors on or off, we modify the atmospheric CO_2, which in turn will have an impact on climate, a feedback neglected in our offline simulations. To place an upper limit on the size of this feedback, we used the atmospheric CO_2 simulated by the NCC experiment (Fig. 3a, dashed line) to force UVic ESCM. In the NCC experiment, ocean carbon uptake is higher, leading to a lower simulated atmospheric CO_2 than the standard SSP5-8.5 scenario (Fig. 3a, solid black line). Compared with the very large changes due to CO_2 emissions, the impact of a lower atmospheric CO_2 on MOC and other parameters is relatively small (Supplementary Fig. 3). This strongly suggests that neglect of carbon–climate feedbacks in the offline simulations is justified.

Change in carbon disequilibrium in response to increasing atmospheric CO_2

In the NCC simulations, both physical and biological disequilibrium components decrease (Fig. 3c). This is a consequence of the slow equilibration timescale of CO_2 such that the rate at which surface ocean carbon equilibrates is slower than the growth rate of atmospheric CO_2. Thus, physical disequilibrium ($C_{dis,phy}$), which is initially negative in high-latitude regions[22] (Extended Data Fig. 2a), becomes more negative over time as the surface ocean diverges from the atmosphere (Fig. 1b and Extended Data Fig. 2b). By contrast, in those same regions, the upwelling of biologically respired CO_2 (refs. 23,38) leads to a positive (total) disequilibrium C_{dis}, which decreases over time (Fig. 1b). Because $C_{dis,bio} = C_{dis} - C_{dis,phy}$, the change ($\Delta$) is given by $\Delta C_{dis,bio} = \Delta C_{dis} - \Delta C_{dis,phy}$. While both terms on the right-hand side are negative, their relative magnitude (and, hence, the sign of $\Delta C_{dis,bio}$) depends on the relative rates of equilibration in the biotic and abiotic models. The equilibration timescale is proportional to $\partial[CO_3^{2-}]/\partial[HCO_3^-]$ in the carbonate chemistry equations, where $[CO_3^{2-}]$ and $[HCO_3^-]$ are the carbonate and bicarbonate ion concentrations, respectively[61]. This derivative is well approximated in terms of the DIC and alkalinity concentrations as (Alk − DIC)/(2 DIC − Alk)[61]. At high latitudes, particularly in the Southern Ocean, DIC is higher in the biotic model owing to upwelling of remineralized carbon, while alkalinity is similar between the two models (Extended Data Fig. 2c). We therefore expect the equilibration time to be shorter in the biotic model than in the abiotic one. This is supported by our simulations (Extended Data Fig. 2d), with the biotic model equilibrating almost twice as fast in the Southern Ocean.

C_{dis} therefore decreases at a faster rate than $C_{dis,phy}$, and $\Delta C_{dis,bio}$ is consequently negative as well. Thus, under increasing pCO_2^{atm}, both physical and biological disequilibria reduce global carbon storage.

Impact of alkalinity redistribution on carbon storage and atmospheric CO_2

Transfer of alkalinity to the deep ocean by sinking particulate inorganic carbon reduces carbon storage[23] because lower surface alkalinity leads to lower DIC at constant pCO_2 (ref. 39). This is reflected in a negative $C_{sat,bio} = -290$ PgC in the PI simulation. A slowing circulation enhances this effect by redistributing alkalinity downwards, making $C_{sat,bio}$ even

more negative. However, at least some of the change in $C_{sat,bio}$ is due to pCO_2^{atm}, which, in our emission-driven simulations, is different for each experiment. We estimate this latter effect in two ways. First, we exploit the corresponding concentration-driven simulations for SSP5-8.5, which are forced by identical prescribed pCO_2^{atm} history (Supplementary Note 1 and Supplementary Fig. 1). In those runs, changes in $C_{sat,bio}$ contribute to ~9% of the total change in C_{sat}, whereas in the corresponding emission-driven run the proportion is ~18%, suggesting that roughly half the change in $C_{sat,bio}$ is due to a redistribution of alkalinity.

As a second, more direct approach, we repeated the emission-driven Circulation experiment with the surface alkalinity field used to calculate CO_2 solubility held at its PI value. As expected, atmospheric CO_2 in this experiment is lower than in the standard Circulation one (Fig. 5b). From the difference between the two experiments, we estimate that, for SSP5-8.5, ~53 ppm of the total change in pCO_2^{atm} of ~94 ppm in 2500 (that is, again approximately half) is due to alkalinity and the remainder due to differences in pCO_2^{atm}.

Ideal mean age

We simulate the ideal mean age as a passive tracer[76] with a surface BC of zero concentration and an interior source of '1' per unit time. In steady state, this tracer can be interpreted as the mean time since a water parcel was last at the sea surface and thus as a measure of the time available for the accumulation of regenerated carbon.

The tracer was first integrated to equilibrium with the PI circulation (Extended Data Fig. 4a), and subsequently from 1765 to 2500 with time-varying circulation for each SSP scenario (Extended Data Fig. 4b–e).

AOU approximation

Apparent oxygen utilization, $AOU = O_{2sat} - O_2$, is the deviation of subsurface dissolved oxygen (O_2) from its temperature-dependent saturation concentration (O_{2sat}). It has been widely used to estimate soft-tissue biological carbon storage $C_{soft,AOU} = R_{C:O}AOU$, where $R_{C:O}$ (0.6364 here) is the carbon to oxygen molar ratio during organic matter respiration[61]. The rationale is that remineralization of organic matter consumes oxygen and thus any deviation of the in situ oxygen concentration from O_{2sat} would indicate respired carbon. However, the underlying assumption of the AOU method that surface ocean oxygen is always at saturation has been proven incorrect. For example, float observations show up to 20% undersaturation in the Antarctic Seasonal Ice Zone[19,77]. This disequilibrium propagates into the interior and leads to large errors in AOU-based estimates of C_{soft} (refs. 11,15–20). In MOBI-TMM, C_{soft} calculated via the carbon decomposition is ~982 PgC for the PI, versus ~1,420 PgC using the AOU approximation, a 45% overestimate. Another study[21] with a data-constrained model of the modern ocean found that AOU overestimates C_{soft} by ~34%. Furthermore, AOU only gives an estimate of soft-tissue carbon storage; it does not include the hard-tissue (C_{caco3}) component of C_{reg}.

Previous studies have also found that AOU-based estimates of changes in C_{soft} can be qualitatively incorrect under large climate shifts[11,19], as also found here (Extended Data Fig. 8a). For the SSP5-8.5 Temperature and Sea ice experiments, C_{soft} calculated using the carbon decomposition increases under global warming, but $C_{soft,AOU}$ decreases. In the Circulation experiment, AOU is reasonably accurate, but when all climate change factors are simultaneously applied, AOU underestimates the true change in C_{soft} and C_{reg} ($= C_{soft} + C_{caco3}$) by ~31% and 47%, respectively, in 2500 (Supplementary Table 2). These errors are even larger for the other emission scenarios and also generally grow with time (Extended Data Fig. 8b).

Data availability

The data required to reproduce the figures shown in this article are available via Zenodo at https://doi.org/10.5281/zenodo.14764349 (ref. 78).

Code availability

The code required to reproduce the figures shown in this article is available via Zenodo at https://doi.org/10.5281/zenodo.14764349 (ref. 78). Model codes are available via Zenodo at https://doi.org/10.5281/zenodo.1246300 (ref. 79) and https://doi.org/10.5281/zenodo.7159021 (ref. 80).

References

62. Muglia, J. & Schmittner, A. Glacial Atlantic overturning increased by wind stress in climate models. *Geophys. Res. Lett.* **42**, 9862–9868 (2015).
63. Muglia, J., Skinner, L. C. & Schmittner, A. Weak overturning circulation and high Southern Ocean nutrient utilization maximized glacial ocean carbon. *Earth Planet. Sci. Lett.* **496**, 47–56 (2018).
64. O'Neill, B. C. et al. The Scenario Model Intercomparison Project (ScenarioMIP) for CMIP6. *Geosci. Model Dev.* **9**, 3461–3482 (2016).
65. Stevens, B. et al. MACv2-SP: a parameterization of anthropogenic aerosol optical properties and an associated Twomey effect for use in CMIP6. *Geosci. Model Dev.* **10**, 433–452 (2017).
66. Khatiwala, S., Graven, H., Payne, S. & Heimbach, P. Changes to the air–sea flux and distribution of radiocarbon in the ocean over the 21st century. *Geophys. Res. Lett.* **45**, 5617–5626 (2018).
67. Eby, M. et al. Lifetime of anthropogenic climate change: millennial time scales of potential CO_2 and surface temperature perturbations. *J. Clim.* **22**, 2501–2511 (2009).
68. Banks, H. T. & Gregory, J. M. Mechanisms of ocean heat uptake in a coupled climate model and the implications for tracer based predictions of ocean heat uptake. *Geophys. Res. Lett.* **33**, L07608 (2006).
69. Yeager, S. & Danabasoglu, G. The origins of late-twentieth-century variations in the large-scale North Atlantic circulation. *J. Clim.* **27**, 3222–3247 (2014).
70. Rugenstein, M. A. A., Winton, M., Stouffer, R. J., Griffies, S. M. & Hallberg, R. Northern high-latitude heat budget decomposition and transient warming. *J. Clim.* **26**, 609–621 (2013).
71. Notz, D. & SIMIP Community Arctic sea ice in CMIP6. *Geophys. Res. Lett.* **47**, e2019GL086749 (2020).
72. Roach, L. A. et al. Antarctic sea ice area in CMIP6. *Geophys. Res. Lett.* **47**, e2019GL086729 (2020).
73. Holmes, C. R., Bracegirdle, T. J. & Holland, P. R. Antarctic sea ice projections constrained by historical ice cover and future global temperature change. *Geophys. Res. Lett.* **49**, e2021GL097413 (2022).
74. Williams, R. G. & Follows, M. J. *Ocean Dynamics and the Carbon Cycle* (Cambridge Univ. Press, 2011); https://doi.org/10.1017/CBO9780511977817
75. Orr, J. C. et al. Biogeochemical protocols and diagnostics for the CMIP6 Ocean Model Intercomparison Project (OMIP). *Geosci. Model Dev.* **10**, 2169–2199 (2017).
76. Holzer, M. & Hall, T. Transit-time and tracer-age distributions in geophysical flows. *J. Atmos. Sci.* **57**, 3539–3558 (2000).
77. Bushinsky, S. M., Gray, A. R., Johnson, K. S. & Sarmiento, J. L. Oxygen in the Southern Ocean from Argo floats: determination of processes driving air–sea fluxes. *J. Geophys. Res. Oceans* **122**, 8661–8682 (2017).
78. Khatiwala, S., Strachan, O. & Schmittner, A. Data and scripts for 'Multi-centennial response of marine carbon pumps to global warming'. *Zenodo* https://doi.org/10.5281/zenodo.14764349 (2025).
79. Khatiwala, S. Transport Matrix Method software for ocean biogeochemical simulations. *Zenodo* https://doi.org/10.5281/zenodo.1246300 (2018).
80. Schmittner, A., Somes, C. J. & Muglia, J. Model code for OSU-UVic2.9-MOBI. *Zenodo* https://doi.org/10.5281/zenodo.7159021 (2022).

Acknowledgements
We thank N. Mengis and S. Fiedler for helpful discussions on generating radiative forcing data for the UVic ESCM simulations.

Author contributions
Conceptualization: S.K. and A.S.; methodology: S.K. and A.S.; investigation: S.K. and O.S.; visualization: S.K. and O.S.; writing – original draft: S.K; writing – review and editing: S.K., A.S. and O.S.

Funding
S.K. discloses support for the research of this work from UKRI (grant nos. NE/W007258/1 and NE/T009357/1), and Waseda University's Global Research Center (GRC) Support Program (project no. GRC-kojin-2503). S.K. also discloses high-performance computing support from the Derecho system sponsored by the US NSF and the University of Oxford Advanced Research Computing facility. A.S. discloses support for the research of this work from US NSF (grant no. 1924215). O.S. declares no relevant funding.

Competing interests
The authors declare no competing interests.

Additional information
Extended data is available for this paper at https://doi.org/10.1038/s41558-026-02686-x.

Supplementary information The online version contains supplementary material available at https://doi.org/10.1038/s41558-026-02686-x.

Correspondence and requests for materials should be addressed to Samar Khatiwala.

Peer review information *Nature Climate Change* thanks Wolfgang Koeve, Neill Mackay and Alban Planchat for their contribution to the peer review of this work.

https://doi.org/10.1038/s41558-026-02686-x

Extended Data Table 1 | Compensation between preformed and regenerated carbon under global warming

2500	SSP1-2.6	SSP2-4.5	SSP3-7.0	SSP5-8.5
Temperature				
ΔC_{pre}	−31.2	−77.7	−186.8	−250.0
ΔC_{reg}	5.2	11	22.9	28.2
ΔC_{total}	−26	−66.7	−163.9	−221.8
$\Delta C_{pre}/\Delta C_{reg}$	−6	−7.1	−8.2	−8.9
Circulation				
ΔC_{pre}	−196.4	−343.5	−670.7	−879.2
ΔC_{reg}	197.7	310.7	432	480.4
ΔC_{total}	1.3	−32.7	−238.7	−398.8
$\Delta C_{pre}/\Delta C_{reg}$	−1.0	−1.1	−1.6	−1.8
All				
ΔC_{pre}	−229.1	−422	−823	−1065.7
ΔC_{reg}	202.2	324.1	459	511.7
ΔC_{total}	−26.9	−97.8	−363.9	−554.0
$\Delta C_{pre}/\Delta C_{reg}$	−1.1	−1.3	−1.8	−2.1
ΔC_{total}(Circ)/ΔC_{total}(Temp)	−0.05	0.49	1.46	1.80

Change (Δ) in the inventory of carbon components in 2500 in the Temperature, Circulation, and All attribution experiments for the four emission scenarios. Changes are with respect to the corresponding No Climate Change experiments. Listed is the change (in PgC) in preformed (ΔC_{pre}), regenerated (ΔC_{reg}) and total (ΔC_{total}) carbon, and the compensation ratio $\Delta C_{pre}/\Delta C_{reg}$. The last row is the ratio of ΔC_{total} in the Circulation experiment to ΔC_{total} in the Temperature experiment.

https://doi.org/10.1038/s41558-026-02686-x

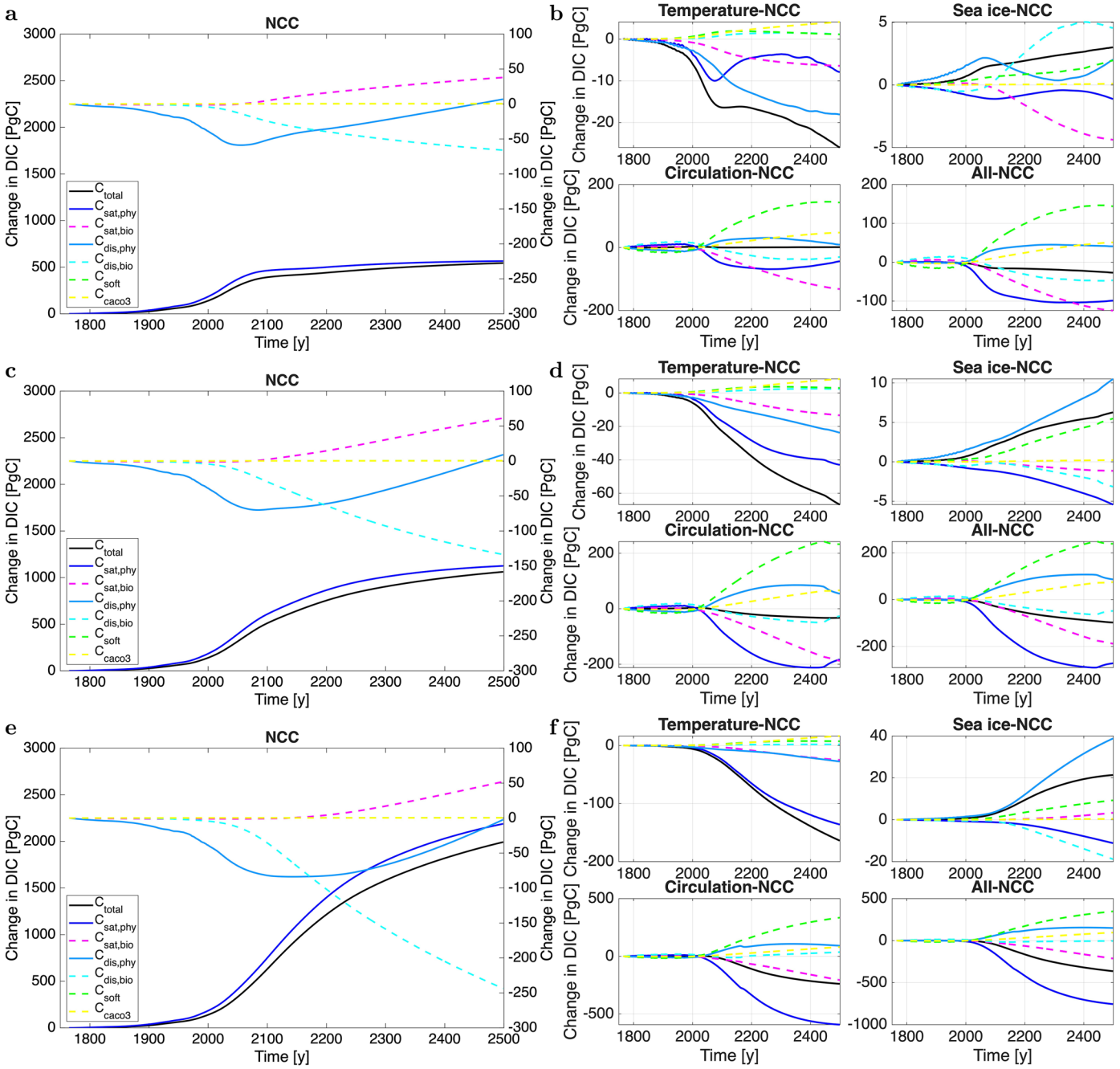

Extended Data Fig. 1 | Evolution of marine carbon components under global warming. (**a**, **c**, **e**) Changes in carbon components in the emission-driven No Climate Change simulations for (**a**) SSP1-2.6, (**c**) SSP2-4.5 and (**e**) SSP3-7.0 scenarios. (**b**, **d**, **f**) Changes in carbon components with respect to NCC in response to different forcing factors for (**b**) SSP1-2.6, (**d**) SSP2-4.5 and (**f**) SSP3-7.0 scenarios (see corresponding left side panels for legends).

https://doi.org/10.1038/s41558-026-02686-x

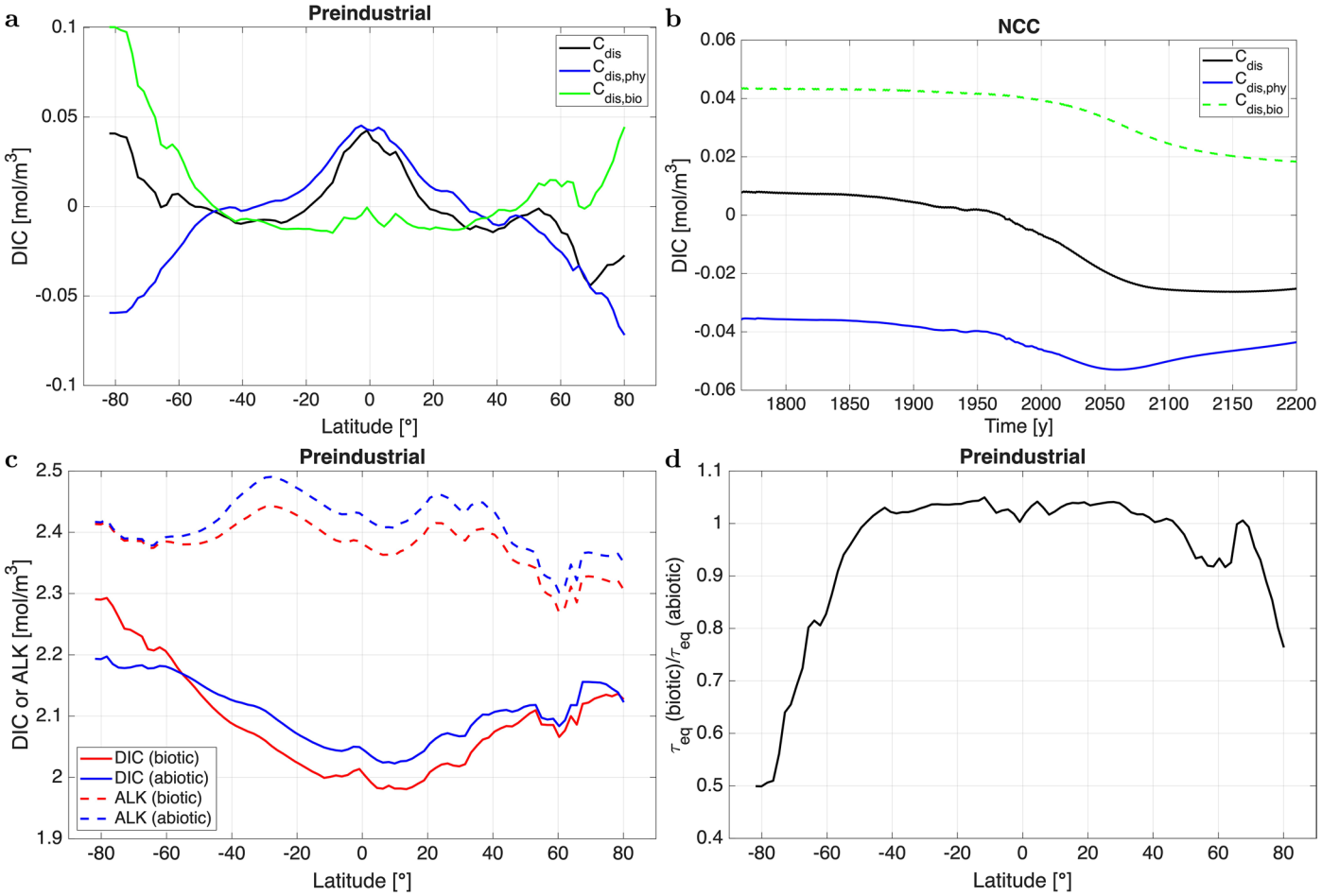

Extended Data Fig. 2 | Disequilibrium carbon. (**a**) Zonal mean surface total (C_{dis}), physical ($C_{dis,phy}$) and biological ($C_{dis,bio}$) disequilibrium components in the PI simulation. (**b**) Time evolution of disequilibrium components averaged over the surface Southern Ocean (<60°S) in the NCC simulation in response to increasing atmospheric CO_2. Disequilibria in this region propagate into the ocean interior, affecting global carbon storage. (**c**) Zonal mean surface DIC and alkalinity in the biotic and abiotic models in the PI simulations. (**d**) Ratio of equilibration times in the biotic and abiotic models based on the approximation described in the text. A more exact calculation using the full carbonate chemistry equations gives nearly identical results.

https://doi.org/10.1038/s41558-026-02686-x

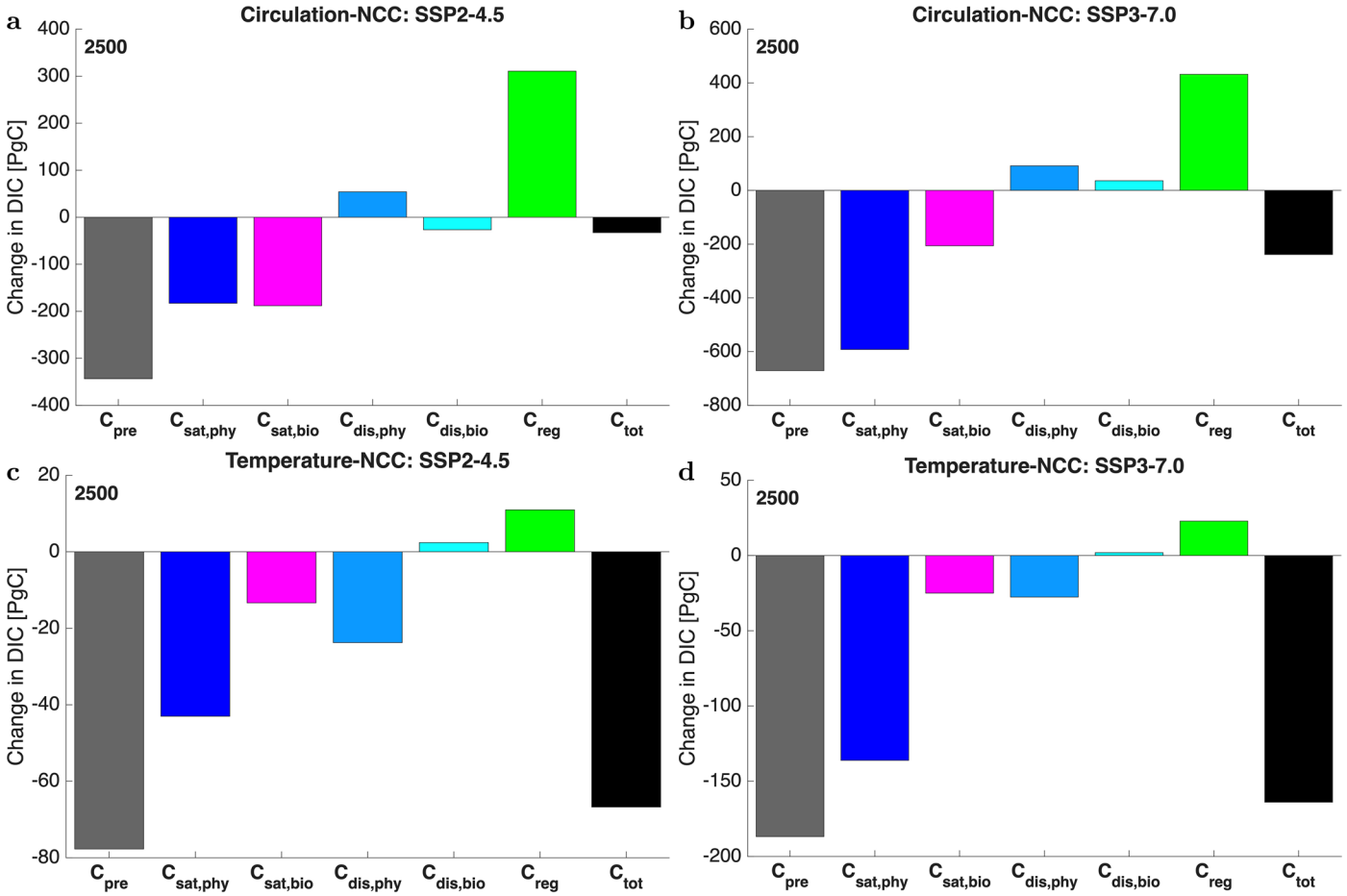

Extended Data Fig. 3 | Impact of circulation and warming on carbon components. (**a**, **b**) Change in carbon components with respect to NCC in year 2500 due to circulation under SSP2-4.5 (**a**) and SSP3-7.0 (**b**). (**c**, **d**) Change in carbon components due to warming under SSP2-4.5 (**c**) and SSP3-7.0 (**d**).

https://doi.org/10.1038/s41558-026-02686-x

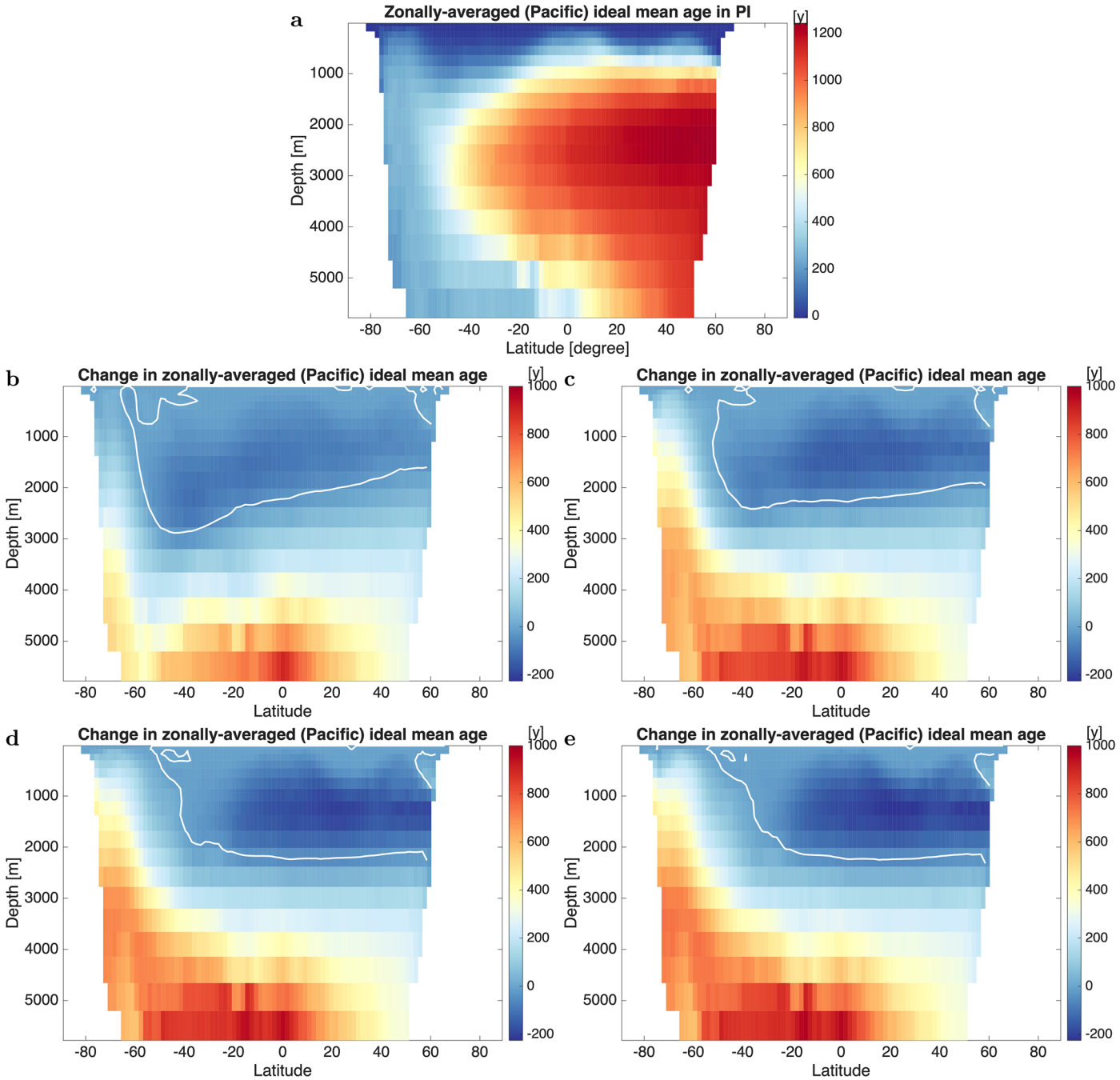

Extended Data Fig. 4 | Ideal mean age under global warming. (**a**) Zonally-averaged section in the Pacific Ocean of equilibrium ideal mean age for the PI circulation. (**b**-**e**) Change in Pacific zonally-averaged ideal mean age between PI and 2500 for SSP1-2.6 (**b**), SSP2-4.5 (**c**), SSP3-7.0 (**d**), and SSP5-8.5 (**e**) scenarios.

https://doi.org/10.1038/s41558-026-02686-x

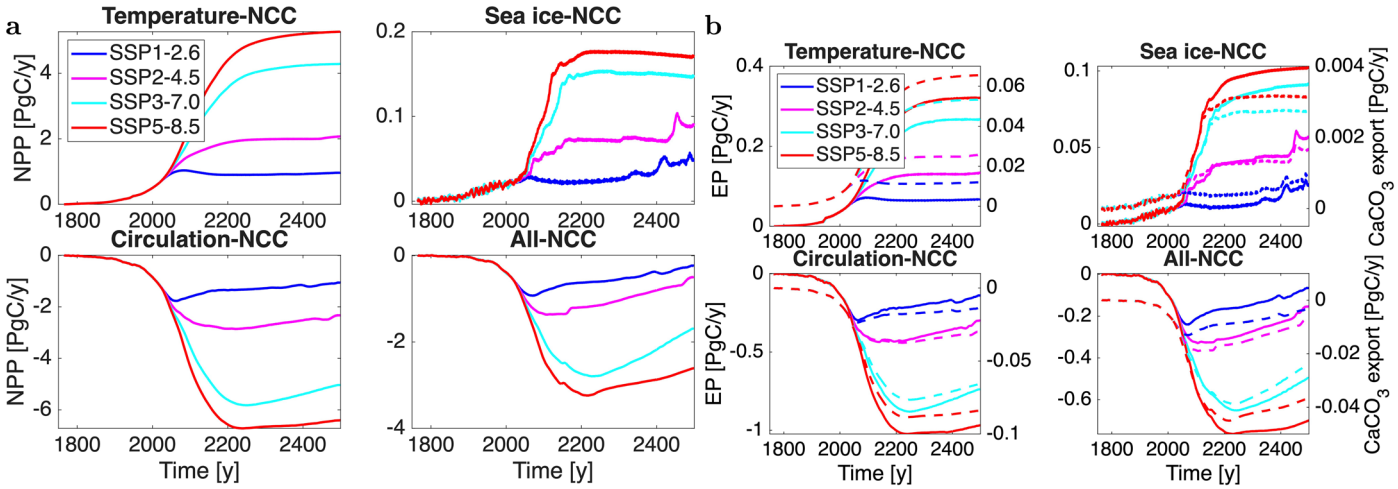

Extended Data Fig. 5 | Primary production and carbon export for different forcing factors and emissions. (**a**) Change in net primary production (with respect to the No Climate Change run) in the attribution experiments for different forcing factors for the four emission scenarios. (**b**) Corresponding changes in export production (solid lines, left axis) and $CaCO_3$ export (dashed lines, right axis).

https://doi.org/10.1038/s41558-026-02686-x

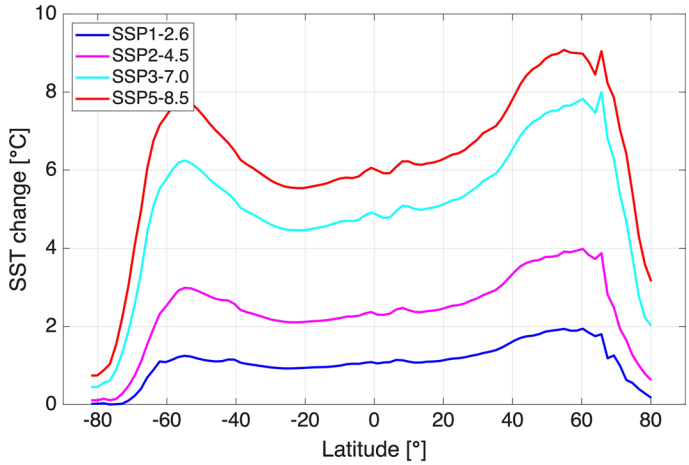

Extended Data Fig. 6 | SST change under global warming. Change in zonally-averaged sea surface temperature (SST) between PI and 2500 for the four emission scenarios.

https://doi.org/10.1038/s41558-026-02686-x

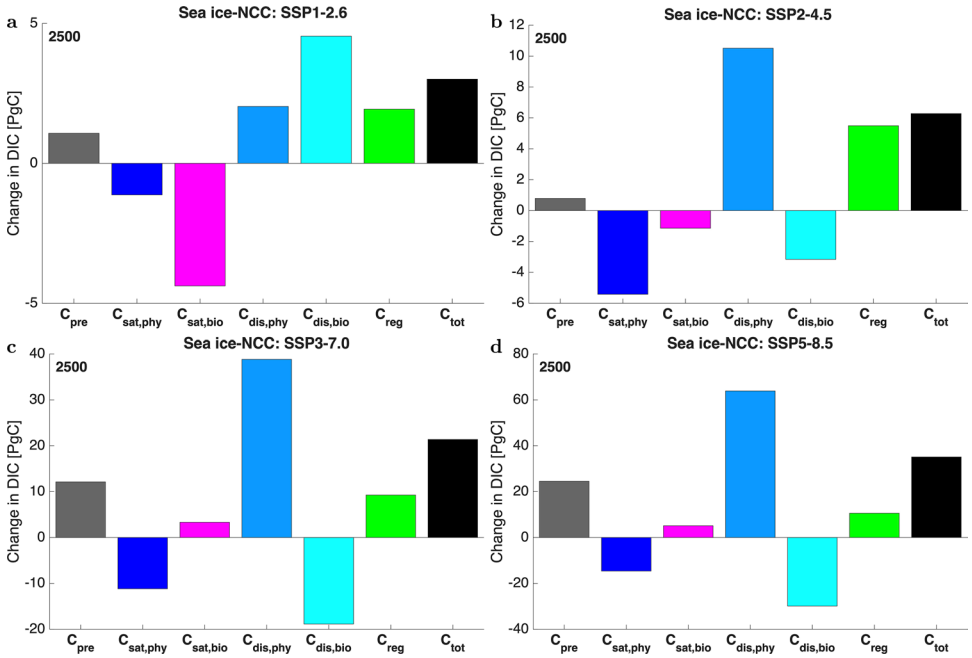

Extended Data Fig. 7 | Impact of sea ice on carbon components. Change in carbon components with respect to NCC in year 2500 due to sea ice for (**a**) SSP1-2.6, (**b**) SSP2-4.5, (**c**) SSP3-7.0 and (**d**) SSP5-8.5.

https://doi.org/10.1038/s41558-026-02686-x

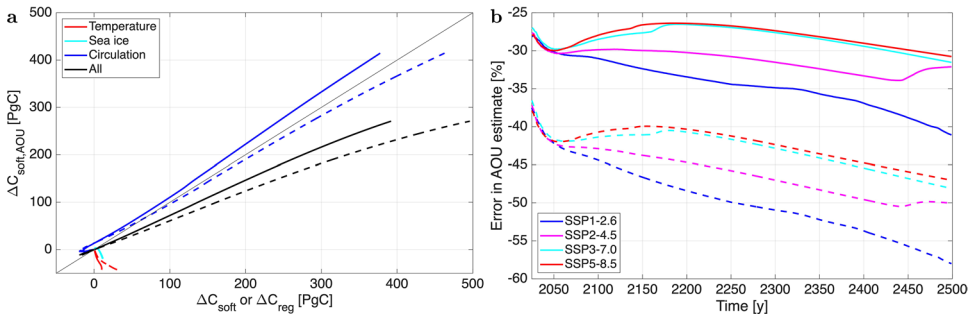

Extended Data Fig. 8 | Apparent Oxygen Utilization. (**a**) Comparison of change (Δ) in C_{soft} estimated using the AOU approximation (vertical axis) with the actual change (horizontal axis) in C_{soft} (solid lines) and C_{reg} (dashed lines) for the various attribution experiments under the SSP5-8.5 scenario. Changes are with respect to the No Climate Change experiment. Each line represents the time-varying, transient solution for the experiment. The grey diagonal line is the 1:1 relationship. (**b**) Relative error (%) between AOU estimate of ΔC_{soft} and true ΔC_{soft} (solid lines) and ΔC_{reg} (dashed lines) in the All experiment as a function of time for the four emission scenarios.

https://doi.org/10.1038/s41558-026-02686-x

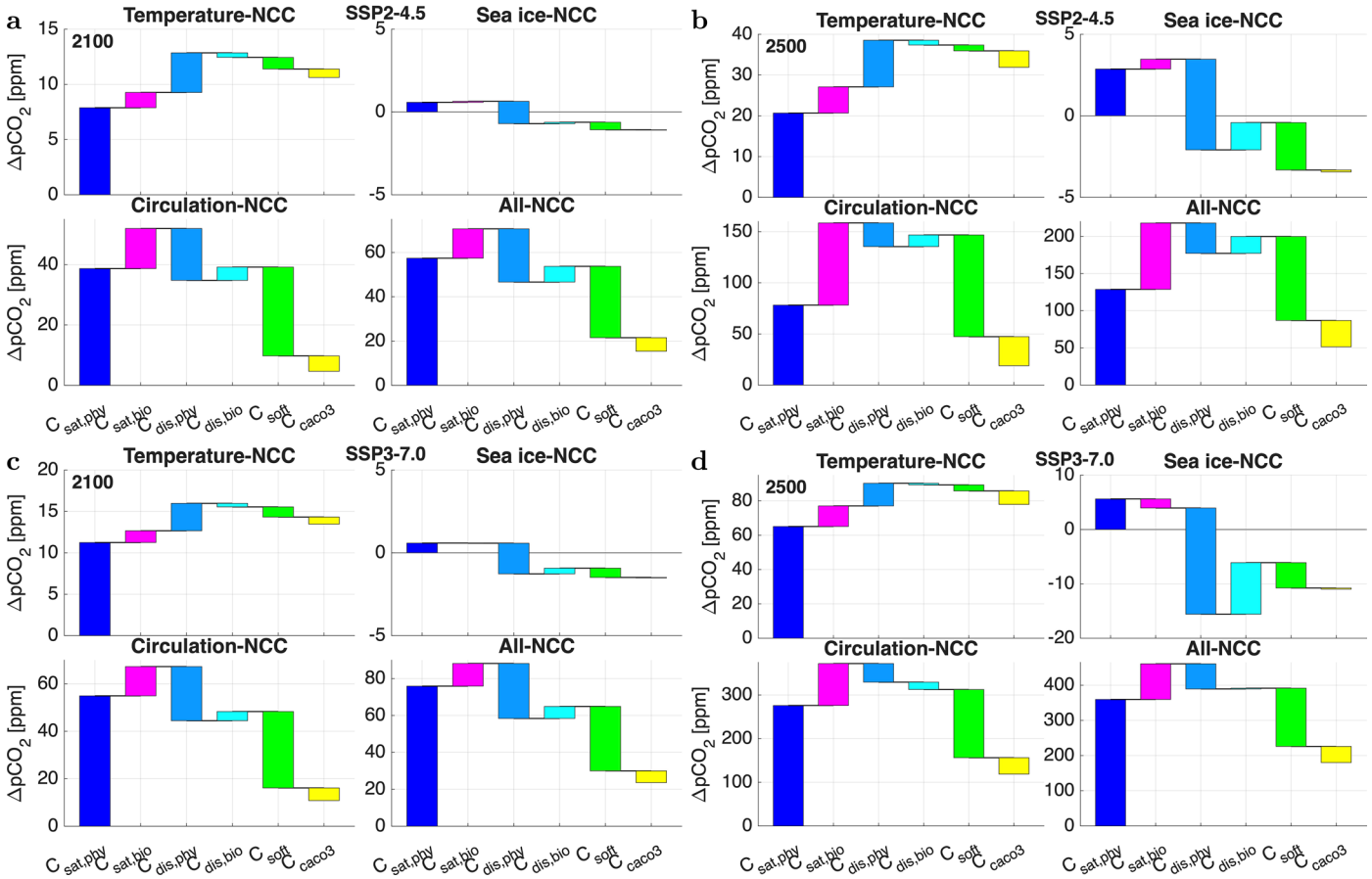

Extended Data Fig. 9 | Impact of marine carbon components on atmospheric CO_2. Waterfall chart attributing changes in atmospheric CO_2 to different carbon components and forcing factors in years 2100 (**a**, **c**) and 2500 (**b**, **d**) for the SSP2-4.5 (**a**, **b**) and SSP3-7.0 (**c**, **d**) emission scenarios.